

submitted to *Geophys. J. Int.*

# **Crustal properties of the northern Scandinavian mountains and Fennoscandian shield from analysis of teleseismic Receiver Functions**

Walid Ben Mansour\*, Richard W. England\*, Stewart Fishwick\*, Max Moorkamp\*

\* *School of Geography, Geology and the Environment, University of Leicester, Leicester, UK.*

*Email: wbm06seismo@gmail.com*

## **SUMMARY**

The presence of high mountains along passive margins is not unusual, as shown by their presence in several regions (Scandinavia, Greenland, East US, SW Africa, Brazil, West India and SE Australia). However, the origin of this topography is not well understood. The mountain range between the Scandinavian passive margin and the Fennoscandian shield is a good example. A simple Airy isostatic model would predict a compensating root beneath the mountains but existing seismic measurements of variations in crustal thickness do not provide evidence of a root of sufficient size to produce the necessary compensation. In order to better constrain the physical properties of the crust in northern Scandinavia two broadband seismic networks were deployed between 2007 and 2009 and between 2013 and 2014. A new map of crustal thickness has been produced from P-receiver function analysis of teleseismic data recorded at 31 seismic stations. The map shows an increase in crustal thickness from the Atlantic coast (38.7 +/- 1.8 km) to the Gulf of Bothnia (43.5 +/- 2.4 km). This gradient in thickness demonstrates

2 *W. Ben Mansour et al. 2018*

that the Moho topography does not mirror the variation in surface topography in this region. Thus, classical Airy isostatic models cannot explain how the surface topography is supported. New maps showing variation in Poisson's ratio and Moho sharpness together with forward and inverse modelling provide new information about the contrasting properties of the Fennoscandian shield and crust reworked by the Caledonian orogeny. A sharp Moho transition ( $R > 1$ ) and low value of  $V_s$  ( $3.5 \pm 0.2 \text{ km.s}^{-1}$ ) are observed beneath the orogen. The shield is characterised by a gradual transition across the Moho ( $R < 1$ ) and  $V_s$  of ( $3.8 \pm 0.1 \text{ km.s}^{-1}$ ) which is more typical of average continental crust. These observations are explained by a Fennoscandian shield underplated with a thick layer of high velocity, high density material. It is proposed that this layer has been removed or reworked beneath the orogen.

**Key words:** Atlantic passive margin, Fennoscandian Shield, Caledonian orogeny, Moho depth, Moho sharpness, Poisson's ratio, crustal density, Isostasy, crustal velocity.

## 1 INTRODUCTION

On the largest scale topography is controlled by lateral and vertical variations in the crustal and lithospheric structure. In most cases, large, long wavelength topographic features are broadly supported by a compensating root. The Scandinavian mountains, which are parallel to a large part of the northeast Atlantic passive margin are a possible exception to this. Previous studies (Ebbing et al. 2005; England & a 2012) have indicated the possible absence of a compensating root beneath these mountains. This raises the question of how this topography is supported and how it formed? Possible mechanisms are magmatic underplating at the time the rifted margin was formed; tectonic compression normal to the margin or upwelling of hot mantle to form the topography in the recent past / present day. These alternatives were discussed by Gallagher (2012) but they have not been tested.

The Scandinavian mountain range is composed of rocks most recently deformed by the Caledonian orogeny which separate the Cenozoic passive margin to the west from the Proterozoic Fennoscandian shield to the east. Apatite fission track and stratigraphic studies appear to suggest that the Scandinavian continental margin underwent uplift of more than 1

*Crustal properties and teleseismic receiver functions* 3

km during the Neogene (Faleide et al. 2002). This may have contributed to the formation of the topography but recent seismic studies of the crust (Svenningsen et al. 2007; Olsson et al. 2008; Stratford & Thybo 2011; England & a 2012; Frassetto & Thybo 2013) have failed to identify a correlation between the high topography of the Scandinavian mountains and variations in crustal properties which can be attributed to relatively recent events. Ebbing & Olesen (2005) suggested that the topography has different origins in the south and the north of the Scandinavian peninsula. In the south, there is some evidence for support resulting from lateral variations in density in the upper mantle whereas in the north the topography appears to be compensated by lateral variations in density in the upper crust (Olesen et al. 2002).

The first seismic studies of the crust beneath Norway and Sweden were refraction profiles; FENNOLORA (Sellevoll & Penttilä 1964; Prodehl & Kaminski 1984; Hossain et al. 1989; Guggisberg et al. 1991; Luosto 1997); and BLUE Road (Hirschleber et al. 1975; Lund 1979; Avedik et al. 1984). These studies showed that the crustal thickness varies between 32 km close to the Atlantic coast to 65 km beneath Finland. More recent refraction profiling studies focussing on the western margin of Scandinavia showed that the thickness of the crust beneath the Scandinavian mountains varies between 38 km and 42 km (Weinrebe 1981; Stratford et al. 2009). In terms of detailed crustal structure and variations in P-wave velocity, the results showed an upper crust 12 to 16 km thick ( $6.0 \text{ km.s}^{-1}$ ), a thick lower crust with a typical velocity of  $6.6 \text{ km.s}^{-1}$  and a transitional Moho (3 to 5 km thick with an average velocity of  $7.2 \text{ km.s}^{-1}$ ). In addition, a low velocity zone at the base of the upper crust was observed in a number of seismic refraction profiles (Lund 1979; Mykkeltveit 1980; Hossain et al. 1989).

The results of the refraction studies were complemented in the 2000's and 2010's with P-receiver function analysis of data collected from a series of broadband passive seismic experiments (Ottemöller & Midzi 2003; Svenningsen et al. 2007; Olsson et al. 2008; England & a 2012; Frassetto & Thybo 2013). Looking at the western Fennoscandian Shield, Ottemöller & Midzi (2003) provided new data on the crustal structure of mainland Norway. They also identified the presence of a low velocity zone at the base of the upper crust and a crustal thickening from 28 km beneath Lofoten Islands to 46 km inland beneath Mo i Rana with a gradual transition from the upper crust to the upper mantle. Olsson et al. (2008) used data from 52 permanent stations to produce a new Moho depth map beneath Sweden, which showed Moho depths of 44 to 48 km beneath the Gulf of Bothnia and estimated the  $V_p/V_s$  ratio for the crust to be between 1.74 and 1.80 in this area. Focussing on the region of high

#### 4 *W. Ben Mansour et al. 2018*

topography in southern Scandinavia, Svenningsen et al. (2007) found a variation in Moho depth from 29 to 32 km on the Atlantic coast to 41 to 43 km beneath the high topography. Extending the previous studies in southern Scandinavia and combining different seismic networks, Frassetto & Thybo (2013) also obtained similar results (25 to 30 km beneath the south eastern Norwegian coast to 35 to 45 km beneath the mountain range). Across the central Scandinavia peninsular, England & a (2012) found crustal thickness varied from 32 km beneath the coast to 43 km beneath the mountain belt. All these results show a crustal thickening from west to east with a crustal thickness of 40 to 45 km beneath the mountain range. However, England & a (2012) also showed that to the east of the mountains, in Sweden, the crust remained at approximately 40 km thick.

The main aim of this study is to image in detail the variation in Moho depth across the northern Scandinavian mountains and Fennoscandian shield using P-receiver function analysis. This study uses data from two temporary broadband seismic networks (31 stations, blue circles and blue triangles of figure 1a) deployed between 2007 and 2009 (SCANLIPS2) and 2013 and 2014 (SCANLIPS3D) across the northern Scandinavian mountains and data compiled from previous studies in this region (Ottemöller & Midzi 2003; Olsson et al. 2008; Silvennoinen et al. 2014). P-receiver functions were computed from multiple teleseismic events recorded at each station and H-k stacking (Zhu & Kanamori 2000) and waveform modelling is used in order to extract 2D crustal models beneath each station. These results are compared with previous models for crustal thickness beneath the region (Luosto et al. 1984; Grad & Luosto 1987; Luosto et al. 1989, 1990; Luosto 1997; Grad et al. 2009). This study results in a new Poisson's ratio map and a Moho map which is an improvement on the large scale, reference models of the European crust produced by Kelly et al. (2007); EuCRUST-07 of Tesauro et al. (2008) and EUNASeis of Artemieva & Thybo (2013).

### **GEOLOGICAL SETTING**

The crust in the region of these seismic experiments (figure 1b) can be divided into two geological domains (Koistinen et al. 2001; Gaál & Gorbatshev 1987). The Caledonian domain across Norway is the result of the last orogenic episode in the North Atlantic region caused by the closing of the Iapetus ocean and the collision between Baltica-Avalonia and Laurentia (Gee et al. 1982). The collision generated a stack of four major allochthonous nappes (Roberts & Gee 1985) with a vergence toward the west. These nappes are composed of late Proterozoic and lower Palaeozoic continental margin rocks and basement metamorphosed to granulite and amphibolite grade (Stephens & Gee 1985, 1989; Grenne et al. 1999; Barnes et al. 2007;

Roberts et al. 2007; Hollocher et al. 2012). In the regions discussed in this paper, the nappes were thrust onto the Norrbotten craton in northern Sweden. This craton lies between the Karelian craton of Archaean age (3.2 - 2.5 Ga) and the Central Svecofennian subprovince formed from a collage of microcontinents and island arcs between 1.85 and 1.66 Ga (Lahtinen 1994; Nironen 1997; Korsman et al. 1999; Korja et al. 2006). A large body of predominantly tonalitic composition at the surface, with a Palaeoproterozoic age of c. 1.8 Ga, the Trans Scandinavian Igneous Belt (TIB), is also present and identified within the NW-SE trending Svecofennian Province and in several places across the Caledonian domain (figure 1b). The origin of the TIB has been debated (Andersson 1997; Åhäll & Larson 2000; Högdahl et al. 2004). Nevertheless, the TIB is suggested to extend north and westwards beneath the mountain range, where it explains the observed gravity and magnetic anomalies (Olesen et al. (2010) and references therein).

## 2 DATA AND METHODOLOGY

### 2.1 SCANLIPS2 and SCANLIPS3D experiments

The SCANLIPS2 (SCANdinavian Lithosphere P and S) and SCANLIPS3D experiments were designed to study the crust beneath the northern and central Scandinavian mountains using arrays of passive seismic instruments recording continuously for up to 18 months. The SCANLIPS2 array was deployed between the end of June 2007 and mid-September 2009 in northern Norway and Sweden (figure 1a). The array consisted of a 450 km long profile with instrument spacing between 30 and 50 km crossing the FENNOLOGRA refraction profiles (Guggisberg et al. 1991) in Sweden. The instruments deployed were 60 and 120 s period broadband sensors with a sampling rate of 50 or 100 Hz. The SCANLIPS3D array, consisting of 20 instruments was deployed south of the SCANLIPS2 profile between the end of June 2013 and mid-September 2014 (figure 1a). The instruments were 60 s period broadband sensors with a sampling rate of 50 or 100 Hz. The BLUE NORMA refraction profile (Lund 1979) crosses the southern part of the network. Seismograms from teleseismic events with a broad range of azimuths and distances were recorded by both arrays.

Teleseismic events with body wave magnitudes greater than 5.8 at epicentral distances between 30° and 100° were extracted from the data and P-receiver functions were calculated from them (figure 2) using the method of Ammon et al. (1990).

6 *W. Ben Mansour et al. 2018*

## 2.2 Computation of P-receiver functions

Since the 1970's a number of workers (Vinnik 1977; Ammon et al. 1990; Langston 1979; Cassidy 1992; Levin & Park 1997; Bostock 2004) developed the P-receiver function technique for imaging seismic discontinuities beneath seismic stations using the converted phases generated at interfaces. This technique is now widely used in seismological studies of the crust and upper mantle. In this study, ZRT (vertical, radial and transverse) receiver functions were calculated using the frequency domain method with a water level deconvolution (Ammon 1991; Clayton & Wiggins 1976; Langston 1979). The deconvolution removes source and propagation path effects from receiver effects after rotating the 3 component waveforms to the backazimuth of the source path. This results in radial ( $E_R$ ) and transverse ( $E_T$ ) receiver functions. The water level is adjusted to the minimum value necessary to stabilize the deconvolution. In this study a mean value of  $10^{-2}$  was selected, which reflects the relatively low signal to noise levels in much of the data. A Gaussian filter of width 2.0 was chosen which corresponds to a centre frequency of 1 Hz. The resulting receiver functions were sorted according to back azimuth and distance (figure 2). Transverse receiver functions were used to identify noisy functions and the possibility of complex dipping structure beneath the station. Receiver functions with anomalous signals and amplitudes were discarded.

## 2.3 H-k stacking analysis

The arrival time of the Ps conversion relative to the direct P-wave and the arrival times of intra-crustal multiples is a function of the ratio of  $V_p$  to  $V_s$  ( $k$ ) and the depth of the Moho ( $H$ ).  $H$  and  $k$  can be estimated using the H-k stacking technique which reduces the ambiguity in velocity ratio and depth to Moho by summing a weighted combination of Ps, PpS and PpSs and PsPs amplitudes along phase moveout curves calculated assuming a single layer over a half space model for the crust for a range of  $H$  and  $k$  values (Zandt & Ammon 1995; Zhu & Kanamori 2000; Niu & James 2002). The peaks in the summation correspond to the most appropriate  $H$  and  $k$  values beneath the station (figure 3). A range of  $H$  values between 35 and 55 km were searched and  $k$  values between 1.65 and 2.0 were chosen on the basis of the available existing geological and geophysical data for the region from previous studies. The procedure used also requires initial  $V_p$  values and weightings of the Ps and multiple phases in the analysis. In this study, an average P-wave velocity between shots F and G along the FENNOLORA profile was used for the initial  $V_p$  value ( $V_p=6.55\pm 0.1$  km.s<sup>-1</sup>). Weightings of (6:3:1) for the Ps, PpS and PpSs and PsPS events were used in fitting the observed arrivals

to those modelled for particular velocity models to ensure that poorly defined multiples did not unduly bias the results of the stacking  $g$  (Zhu & Kanamori 2000).

From the H-k stacking results it is also possible to obtain an indication of average crustal composition from an estimation of Poisson's ratio calculated from the best fit estimate of  $V_p/V_s$  (Chevrot & van der Hilst 2000). Poisson's ratio typically varies between 0.20 and 0.35 and is sensitive to the presence of fluids and the crustal mineralogy (mafic vs felsic). For example, a high Poisson's ratio ( $\sigma > 0.3$ ) can be interpreted as the presence of fluid (Watanabe 1993), low silica content (Musacchio et al. 1997) or anisotropy effects (Hughes et al. 1993; Wang et al. 2012). Variation in both Poisson's ratio and crustal thickness can be associated with geological features. For example, in Australia the Proterozoic crust generally shows higher values of Poisson's ratio and crustal thickness than the Phanerozoic crust (Chevrot & van der Hilst 2000).

Where stacks of receiver functions did not exhibit clear multiples the uncertainties in the results of H-k stacking are greater. Where this occurred, the crustal thickness was estimated by increasing the weighting of the Ps-delay time relative to the multiples and  $V_p/V_s$  ratios were assumed to be similar to adjacent seismic stations. Precision in determining the estimate of Moho depth depends on the correct estimation of the arrival time of the Ps conversion and the first multiple (PpS). Generally, uncertainties in the Moho depth are of the order of 2 to 3 km (figure 3) where there is a sharp transition between the lower crust and upper mantle. Larger uncertainties are seen where a transitional Moho is suspected.

#### **2.4 Moho Sharpness**

An analysis of the amplitude of the converted phases in receiver functions can provide information on the contrast in the change in velocity between the lower crust and the upper mantle. The sharpness of the Moho beneath a station can be quantified as the ratio of the amplitude of the Ps phase to the amplitude of the direct P-wave arrival on the SV component of the seismogram (Owens et al. 1984). Primarily, the amplitude of the Ps phase depends on the contrast in P-wave to S-wave velocity across the Moho which determines how much energy is transmitted as a converted S-wave. A small contrast in velocity will result in a low amplitude S-wave and a low Ps/P amplitude ratio. A large contrast in velocity will result in a high amplitude S-wave and hence a high Ps/P amplitude ratio. The amplitude of the Ps phase can also be affected by the incidence angle of the teleseismic event at the base of the crust. When the angle is large the amplitude of the Ps conversion is also large. However, its

8 *W. Ben Mansour et al. 2018*

effect can be overcome by taking an average value of the Ps/P ratio for each station which will be associated with an average incident angle.

Youssof et al. (2013) calculated LQT receiver functions and suggested using a regional average for the Ps amplitude for the whole array as a reference value. This approach allows for identification of small scale variations in velocity structure suggested by local variability in amplitude ratios. Here, we use a similar approach but use ZRT receiver functions and Moho sharpness is computed beneath each station by normalizing the Ps/P ratio for each P-receiver function by the average value of the Ps/P ratio for the whole array across the northern Scandinavian mountains and the Fennoscandian shield.

Moho sharpness  $>1$  suggests that the reference value is smaller than the ratio of Ps/P and hence the velocity contrast is large and the Moho transition is sharp. A Moho sharpness of  $R < 1$  suggests a weak velocity contrast and a gradual transition.

Here, this approach is used to quantify the Moho sharpness (R) across the northern Scandinavian mountains and the Fennoscandian shield. The SCANLIPS2 and SCANLIPS3D experiments recorded teleseismic waves with a large range of slowness values which provide a reliable estimation of Moho sharpness in this region.

## 2.5 Waveform and shear wave modelling

Forward modelling provides an initial guide to the velocity structure to be used in an inversion. It can also be used to test a variety of velocity models to determine how closely synthetic waveforms generated from these models approximate the observations. Several initial models were tested to provide an initial estimate of  $V_p$ ,  $V_s$  and depth based on the FENNOLORA profile for each station in the SCANLIPS2 array and the SCANLIPS3D network. Synthetic 3 component waveforms for each station were calculated from the initial models using the respknt code written by Randall (1994). These were processed in the same way as the real data for each velocity model to produce synthetic receiver functions. The synthetic receiver functions were then compared with the observations. Greater emphasis was placed on obtaining a good match between peaks and troughs (Ps and the multiples) than attempting to compare amplitudes. Modification of the velocity model was necessary to optimise the fit between the synthetic and observed receiver functions. This provided an estimate of possible values for the Moho depth, velocity structure and the most appropriate  $V_p/V_s$  ratio. Successful modelling of the amplitudes of the observed arrivals requires a broader investigation of the range of possible variations in  $V_p/V_s$  ratio and velocity structure

beneath each instrument than can be undertaken through forward modelling and this is best achieved by inverse modelling.

Inverse modelling of receiver functions involves converting arrival times and amplitudes of phase conversions / multiples in a time series into a shear wave velocity model in depth. The inversion is complicated by the non-linear relationship between the data and the model parameters. The travel time of an individual Ps conversion is dependent on the depth of the interface and on the S-wave velocity above the interface (Ammon et al. 1990). The inversion seeks to minimise the difference between the observed and model generated receiver functions. Layer thicknesses, which are held constant within the inversion scheme, are initially based on the results of forward modelling. Increasing the number of layers and decreasing their thickness (to an estimated minimum resolvable thickness of c. 2 km) can be used to attempt to characterise the velocity gradients within the crust. The initial Vp/Vs ratio is based on the H-k stacking results and constrains the average value for the whole crust.

### 3 RESULTS

#### 3.1 P-Receiver Functions

This study uses 235 P-receiver functions from events recorded between 2007 and 2009 and 415 events recorded between 2013 and 2014.

Table 1 in the appendices summarizes key information for each seismic station (latitude, longitude, elevation, sensor type) together with the number of P-receiver functions for each station used in this study. Eighty percent of the events used originated from the Pacific rim but others recorded from the Atlantic, Mediterranean, Africa and the Indian Ocean have been used. The stations have been classified as poor, medium and good based on the number of teleseismic events yielding usable receiver functions recorded in 4 geographic quadrants. A station is good if there are 1 or more useable receiver functions from each quadrant; medium if receiver functions are available from 3 quadrants. Otherwise the station is classed as poor. 11 stations are classed as good, 15 medium and 5 poor.

For each station, the receiver functions were sorted by back azimuth and stacked into 5 degree bins. Stacking enhanced the clarity of the Ps conversion (Moho conversion) at 5 +/- 1 s and the crustal multiples (PpS and PsPs).

For example, station 7001 shows relatively consistent Ps and PpS arrivals across a range of backazimuths (figure 2). Furthermore, the stacked radial receiver function, for this station

10 *W. Ben Mansour et al. 2018*

shows a good signal to noise ratio. Unfortunately, most of the receiver functions show low amplitude crustal multiples and stacking does not significantly improve the signal to noise ratio. For example, station 1307, classified as poor, shows a low amplitude Ps conversion but has a relatively clear PpS multiple in the individual and stacked radial functions (figure 2). This could be explained by a low velocity contrast between the upper mantle and the lower crust (Niu & James 2002; Thurner et al. 2015) and / or a dipping Moho (Cassidy 1992; Savage 1998; Lombardi et al. 2008).

Along the SCANLIPS2 array the delay between the Ps conversion and the direct P wave arrival increases from station 7001 on the Atlantic coast (4.9 s) to station 7027 (5.3 s) on the coast of the Gulf of Bothnia. However, the suggestion of a gradual increase in delay time is misleading. There are considerable variations in delay time along the length of the profile (figure 4). The maximum delay time appears to be 6.6 s, for events arriving beneath station 7017 located on the Norbotten craton close to the intersection with shots F and G of the FENNOLOGRA experiment (figure 1). The Ps delay times recorded on stations of the SCANLIPS3D array in the south, within the region affected by Caledonian orogenic events are typically greater (6.0 +/- 0.5 s) than those recorded in the north along the SCANLIPS2 array which are comparable to the delays recorded at stations deployed on the shield. However, a compilation of Ps-P delay times recorded at stations in both deployments confirms an overall increase in delay times from the Atlantic coast to the Gulf of Bothnia.

### 3.2 Moho depth and Poisson's ratio

To reduce the ambiguity between depth and velocity the H-k stacking technique (Zhu 2000) was used on data from each station. The technique is sensitive to shear wave velocity, so P-wave velocity in the crust is held constant and variations in velocity described in terms of the  $V_p/V_s$  ratio. Knowledge of the P-wave velocity in this region is limited to the results of the FENNOLOGRA experiment across the Fennoscandian shield (Prodehl & Kaminski 1984; Guggisberg et al. 1991; Luosto 1997). This experiment modelled the crust as a two-layer structure and constrained the average P-wave velocity in the upper crust to 6.1 +/- 0.1 km.s<sup>-1</sup> and to 6.9 +/- 0.2 km.s<sup>-1</sup> in the lower crust in the area where it crosses the SCANLIPS2 array (between shots F and G of the FENNOLOGRA profile). Using these data a weighted average P-wave velocity for the crust of 6.55 +/- 0.1 km.s<sup>-1</sup> was calculated but in order to consider the uncertainty in the choice of P-wave velocity 3 values (6.45, 6.55 and 6.65 km.s<sup>-1</sup>) were tested. Table 2 in the appendices summarizes the results of H-k stacking for each station

(thickness and  $V_p/V_s$  ratio) using a  $V_p$  value of  $6.55 \text{ km.s}^{-1}$ , which gave the most stable results.

Results of H-k stacking in figure 3 show a complex structure of the crust beneath the seismic stations. By selecting a reasonable range of values in depth (34-50 km) and  $V_p/V_s$  (1.64-1.90) in Scandinavia and a P-wave velocity of  $6.55 \text{ km.s}^{-1}$  we isolate the best pair of H and  $V_p/V_s$  values. In most cases only one pair of values is identified (figures 3.a and 3.e). However, beneath some stations such as stations 7023 and 7025 (figures 3.b and 3.c) show a second peak located at the top of the normalised area (in blue rectangle on figure 3) is present. These unrealistic values of H ( $> 50 \text{ km}$ ) and  $V_p/V_s$  ( $< 1.70$ ) suggest complex crustal structure beneath the station which affect the energy of the arrivals in the receiver function.

Four stations from seven of those deployed on the Fennoscandian shield during the SCANLIPS2 experiment do not show a clear crustal multiple (PpS conversion) after stacking of individual receiver functions with obvious PpS conversions. Consequently, the Moho depth is poorly constrained for these stations. However, a comparison with values of Moho depth at nearby stations (SAL, DUN, ERT) from previous receiver function studies (Olsson et al. 2008) and the FENNOLORA profile enable an estimate of Moho depth without the presence of this crustal multiple for these stations. For example, analysis of receiver functions at station ERT, 20 km from 7020, shows a weak variation of Moho depth between these two stations ( $H_{ERT} = 41.9 \text{ km}$  and  $H_{7020} = 43.5 \text{ km}$ ). For the station 7025, we use closest station (station 7023 located at less than 20 km) to validate the values estimated from H-k stacking ( $H_{7023} = 42.9 \text{ km}$  and  $H_{7025} = 43.1 \text{ km}$ ).

Along the SCANLIPS2 array crustal thicknesses estimated from H-k stacking increase from west to east, from 41.5 km beneath station 7001 to 44.1 km beneath station 7027. The northern part of the SCANLIPS3D network (stations 1304, 1307, 1308, and 1311) and the station furthest west (1301) show the highest values of Moho depth (46 to 48 km). Overall, values of Moho depth are more variable beneath the Caledonian domain than beneath the Fennoscandian Shield. Uncertainties in the estimation of Moho depth are greater from stations in the SCANLIPS3D network than the SCANLIPS2 array (Figure 5).

The H-k stacking method also provides constraints on the mean Poisson's ratio of the crust, based on the calculated  $V_p/V_s$  ratio. The results yield values in the range 0.27 to 0.32 along the SCANLIPS2 array and a range of 0.26 to 0.34 in the SCANLIPS3D network. These values are high relative to the average value of 0.25 for continental crust cited by Zandt & Ammon (1995). Figure 6 shows the Poisson's ratio for all the instruments plotted against distance from the Atlantic coast (which is also parallel to the edge of the Caledonian orogen).

12 *W. Ben Mansour et al. 2018*

This plot shows that the mean value of Poisson's ratio for the Caledonian domain ( $\sigma = 0.29 \pm 0.02$ ) and for the Fennoscandian Shield ( $\sigma = 0.28 \pm 0.02$ ) are very similar. A plot of  $V_p/V_s$  ratio against Moho depth shows no correlation between these two variables ( $R^2 = 0.01$ ) (figure 6). In addition, estimates of Moho depth, mean  $V_p/V_s$  ratio and Poisson's ratio from previous studies were compiled to plot a series of maps showing the variation of these properties across the region (figure 7 and Appendix Table 2). The new data fill significant gaps in existing maps, (Luosto 1997; Grad et al. 2009) providing better constraints on the properties and thickness of the crust in northern-central Norway and northern Sweden.

The map of Moho depth suggests that there is considerable variation in the thickness of the crust beneath both the Caledonian domain and the Fennoscandian shield. The new data also show that the crust is relatively thick along parts of the Atlantic coast. The compilation of Moho depth estimated from the controlled source experiment ( $H=45$  km, yellow star on figure 5) and values estimated from P-receiver function analysis along the SCANLIPS2 array shows a deeper crust (5-6 km) in the shield, west of the intersection between the FENNOLORA profile (yellow star on figure 5) and the SCANLIPS2 (stations N7017 and N7018).

The Poisson's ratio map on figure 7b shows high values of Poisson's ratio ( $\sigma = 0.28 - 0.33$ ) on the Atlantic coast and a region with relatively lower values ( $\sigma = 0.25 - 0.30$ ) beneath the mountain range in the northern part of SCANLIPS3D array and higher values ( $\sigma = 0.30 - 0.32$ ) in the southern part. Across the shield area there are two trends. Low values ( $\sigma = 0.25 - 0.27$ ) are recorded beneath the eastern part of the SCANLIPS3D network and higher values are seen to the north beneath the SCANLIPS2 array. These variations will be discussed below.

### 3.3 Moho sharpness

To calculate the Moho sharpness ( $R$ ) for each station, a  $P_s/P$  amplitude ratio was calculated and then an average value ( $R_{mean} = 0.275$ ) combining stations from SCANLIPS2 and SCANLIPS3D experiment was determined and used as reference value for the study area. A normalised value of Moho sharpness greater than 1 is interpreted as indicating a relatively strong velocity contrast between the upper mantle and the lower crust and a normalised value of less than 1 is interpreted as a relatively weak velocity contrast and a gradational transition between the crust and upper mantle. Table 2 in the appendix summarises the Moho sharpness values for each station and the results are plotted in figure 8.

Two domains can be identified from the relative Moho sharpness ( $R$ ) values across the

study area. Beneath the Caledonian domain  $R$  is generally above 1 with values which vary from 1.0 to 1.4, except beneath stations 1308 ( $R = 0.81$ ), 1303 ( $R = 0.87$ ), 1320 ( $R = 0.83$ ), 7014 ( $R = 0.89$ ) and with no linear trend from west to east. Beneath the shield relative Moho sharpness varies between 0.61 (station 7023) and 0.84 (station 7020). Except station 1321 ( $R = 1.06$ ) all values are less than 1, with no linear trend from west to east (figure 8).

By interpolating available values for relative Moho sharpness, a 2D Moho sharpness map in this region has been produced (figure 8). This map indicates that, generally, beneath the Caledonian domain the transition between the lower crust and the upper mantle is relatively sharp (Relative  $R < 1$ ) and it is more gradational beneath the Fennoscandian shield (Relative  $R < 1$ ).

### **3.4 Waveform and shear wave modelling**

In the preceding sections H-k stacking and determination of relative Moho sharpness has been used to determine the first order properties of the crust beneath each station. In order to better constrain the variation in velocity with depth beneath each station forward and inverse modelling of the P-receiver functions was undertaken. This also addresses two aspects of the crustal properties identified by previous studies in the region. Firstly, Mykkeltveit (1980), Hossain et al. (1989) and Ottemöller & Midzi (2003) suggested the presence of a low velocity layer at the base of the upper crust. Secondly, the presence of magmatic underplating (of undetermined age) has been suggested by previous studies across the southern part of the Scandinavian peninsular (Thybo 2001; Stratford & Thybo 2011; England & a 2012)

Three crustal velocity models derived from previous studies in Scandinavia were tested as starting models for determining crustal velocity structure. Model 1 (Black curve in figure 9a) is derived from the FENNOLORA experiment. This model has 3 layers with a sharp transition between the crust and the upper mantle. Model 2 is based on the studies of (Mykkeltveit 1980; Hossain et al. 1989; Ottemöller & Midzi 2003) and has a low velocity zone (LVZ) at the base of the upper crust. Finally, model 3 is similar to model 2 but with a gradational transition from the low velocity layer to the thin high velocity layer at the base of the crust (Blue curve in figure 9a). Synthetic seismograms for these models were generated using the respknt code of Randall, based on the reflection matrix method developed by Kennett (1983). These seismograms were then used to calculate synthetic receiver functions using the frequency domain method of Ammon et al. (1990), as described above.

Figure 9 shows a comparison of the synthetic receiver functions calculated from each

14 *W. Ben Mansour et al. 2018*

model against examples of real receiver functions. There is a broad match between the amplitude of the direct P wave and the Ps conversion. This suggests the models for the velocity of the crust and the velocity contrast between the lower crust and upper mantle are a reasonable approximation to the actual crustal structure. However, an upper crustal conversion between the direct P-wave and the Ps conversion is not observed beneath every station in the data. For example, station 7001 located close to the Atlantic coast does not show this feature. Station 7023 on the shield shows an upper crust conversion at c. 2 s after the direct P-wave arrival associated with an increase in velocity with depth. The data do not match the synthetic seismograms derived from the model containing a low velocity zone suggesting that velocity increases with depth beneath all the stations (figure 9).

To explore a larger range of models of varying crustal velocity with depth that are consistent with the observations, inverse modelling of P-receiver functions was conducted following the approach of Moorkamp et al. (2010). This method was previously applied to data from the Slave and Kaapvaal Cratons and uses the multi-objective genetic algorithm (GA) NGA II of Deb et al. (2002). The parameterization of the model involves specifying the minimum value (thickness, shear velocity) for each layer, the size of discretization of each layer and the number of bits needed for encoding the thickness and the shear wave velocity. The GA runs with a population size of 1000 for 500 iterations to ensure that a new generation of models is produced according to the criteria of dominance in nature by using the concept of Pareto optimality (Corne & Knowles 2007). The optimum model selected for each iteration corresponds to the minimum rms misfit and minimum smoothness obtained from L-curve analysis (Hansen 1992).

Comparisons between real and synthetic P-receiver functions for each station do not show a change in polarity at between 1 and 3 s after the direct P-wave, when the arrival of a conversion associated with the presence of a low velocity zone at the base of the upper crust is expected. For example, station 7023, located on the Fennoscandian shield, does show a conversion from an upper crustal layer but this is associated with increasing velocity with depth rather than a decrease (figure 9). Consequently, it is concluded from the results of the inverse modelling of the receiver functions that the low velocity layer identified in previous studies (Mykkeltveit 1980; Hossain et al. 1989; Ottemöller & Midzi 2003) is not required in our models to explain our observations.

The contrast in velocity across the Moho (or Moho sharpness) was also investigated using the results of the inverse modelling. As noted above (section 3.3), there is a contrast in Moho sharpness between the Caledonian domain and the shield area. In previous work

(Thybo 2001; Stratford & Thybo 2011; England & a 2012) across the Fennoscandian shield the transition between the lower crust and the upper mantle is interpreted as being composed of a 3 to 6 km thick high velocity ( $V_p > 7.0 \text{ km.s}^{-1}$ ) layer. Figure 10 shows a range of inverse models (velocity vs depth) from different stations plotted according to whether they were deployed on the shield or the Caledonides. Comparatively few stations beneath the Caledonian domain have optimum velocity depth models containing a thick high velocity layer at the base of the crust. This is in contrast to the stations deployed on the shield. These results are consistent with the results of the study of Moho sharpness which suggested that there is a small contrast in velocities above and below the Moho beneath the shield (relative  $R < 1$ ) and a strong contrast in velocity across the Moho beneath the Caledonian domain. They are also consistent with maps of the velocity structure for Scandinavia (e.g. Laske et al. (2013) and Tesauro et al. (2008)) but these maps are based on relatively limited amounts of data.

#### 4 INTERPRETATION AND DISCUSSION

This regional study of the crust, using 2 arrays across northern Norway and Sweden, provides new information about its present-day properties (thickness, Moho sharpness and shear wave velocity). The region consists of the Fennoscandian shield and the Caledonian orogenic domain, which is composed of tectonically reworked shield and deformed late Proterozoic and lower Palaeozoic continental margin rocks.

From the H-k stacking results the shield shows an average crustal thickness of 45 km (range 41 to 49 km). This value is at the upper end of the global average thickness of 41.5 (+/- 5.9) km beneath all Precambrian shield areas, as determined by Christensen & Mooney (1995). Abbott et al. (2013) presented a detailed study of the Moho characteristics beneath Archean crust of different stabilisation ages. In the area studied here, the Fennoscandian shield is thought to have a stabilisation age of 2.5 to 2.6 Ga Gorbatshev & Bogdanova (1993); Mikkola et al. (2011); Mänttari & Hölttä (2002). However, the mixture of crustal units across the shield, an absence of sedimentary rocks and later Proterozoic tectonothermal reworking along the southern edge of the shield make estimating the actual stabilization age difficult. In comparison with shield areas showing the same or similar stabilization age, the results from the two arrays indicate that the shield displays unusually thick crust, as previously suggested by Olsson et al. (2008) for Sweden and Kozlovskaya et al. (2008) for Finland. In comparison, the Yangtze craton in south China and the North China craton show very

16 *W. Ben Mansour et al. 2018*

wide ranges of crustal thicknesses (32 to 48 km), while the Slave craton in North America, the Sao Francisco craton in South America and the Aravali-Bundellkhand craton in India have generally thinner crust (36 to 43 km) (Abbott et al. (2013) and references therein). The Caledonian domain shows an average crustal thickness of 42 km and a range of (39 to 44 km). These values indicate the crust is slightly thinner than beneath the Fennoscandian shield, despite it having been thickened as a result of contractional deformation during the Caledonian orogeny. This can be reconciled either by the amount of thickening of the crust not reversing the extension and thinning to form the continental margin from which the orogen has been built or thinning by post-orogenic extensional collapse.

From modelling of P-receiver functions, the average  $V_s$  velocity for the crust across the shield ( $V_s = 3.8 \pm 0.1 \text{ km.s}^{-1}$ ) is consistent with the average value of continental crust of  $3.7 \text{ km.s}^{-1}$  (Christensen & Mooney 1995) and the value of Hyvönen et al. (2007) and Kozlovskaya et al. (2008) in Finland beneath the central Fennoscandian shield ( $V_s = 3.6$  to  $4.2 \text{ km.s}^{-1}$ ). The inverse modelling of velocity structure and the H-k stacking suggests the presence of a high velocity layer at the base of the lower crust beneath the shield (figure 10). The results of the study of Moho sharpness show that the values for the shield are low, which is consistent with the observed velocity structure, in which the high velocity lower crust shows a small contrast in velocity with the underlying upper lithospheric mantle immediately below the Moho.

The low value of Moho sharpness beneath the shield is largely the result of the presence of a high velocity layer at the base of the crust. The presence of this high velocity lower crustal layer beneath the shield and the transition to higher values of Moho sharpness between the Shield and the orogen could be explained by a number of simple models. First, the high velocity layer at the base of the crust formed only beneath the shield. Second, the high velocity layer originally extended beneath the whole of the region and has been selectively removed from beneath the orogen. Third, the high velocity layer could be an artefact of the approach taken in analysing the data. However, England & a (2012) found a similar high velocity lower crustal layer beneath the Shield but not beneath the orogen in a profile crossing central Norway and Sweden, suggesting that the observations made in this study are consistent with previous work and that it is unlikely that the observations are an artefact of the data analysis. Beneath southern Scandinavia, Stratford & Thybo (2011) and Kolstrup & Maupin (2013) describe the presence of a thick layer of high velocity material at the base of the shield which thins west of the Oslo graben and beneath the Caledonian orogenic belt. The observations of the transition in R values is also relatively consistent in

the data presented here, which suggests that the observation is not an artefact. The most common interpretation of these lower crustal high velocity layers is that they are formed by magmatic underplating, or that they are eclogite (Kukkonen et al. 2008). In this case the  $V_p/V_s$  ratio observed beneath seismic networks are higher than expected for the presence of eclogite ( $V_p/V_s$  1.77-1.78, Thompson et al. (2010) and reference therein). The absence of a high velocity layer at the base of the crust could be the result of delamination of an eclogitised lower crust beneath the orogen (Austrheim et al. 1997).

Before the Caledonian deformation took place the shield area must have undergone significant exhumation such that its surface exposed moderate to high grade metamorphic rocks. A considerable amount of erosion is required over a large area to expose moderate to high grade metamorphic rocks at the surface and this cannot be achieved only by erosion of an orogenic belt (Platt 1993). Therefore, the most likely cause of this erosion is uplift due to magmatic underplating, which is consistent with the presence of the high velocity layer at the base of the crust. If the exhumation of the shield was caused by underplating at least part of the underplating predates the Caledonian deformation because Caledonian nappes rest directly on the exhumed moderate to high grade metamorphic rocks. This would mean the underplating/high velocity layer originally extended beneath at least parts of the orogen and that it was subsequently removed by delamination or reworked into the middle and lower crust during deformation of the edge of the shield associated with the Caledonian orogenic event. The remaining possibility, that the high velocity layer was formed only beneath the shield, is considered unlikely given that previous studies along the length of the orogen have consistently noted that the high velocity layer is found only to the east of a line corresponding to the strike of the orogen. There is no process which could easily explain this relationship.

Similar relationships between shields and adjacent orogens have been observed elsewhere, suggesting that the process of modification of the crust postulated here is a common feature of crustal evolution. In South America, the Sao Francisco craton (38-43 km thick) is surrounded by thinner ancient orogenic belts (Brazilia and Ribeira, 34 to 42 km thick) and in China, the Yangtze craton (31 to 46 km thick) has a common margin with the thinner (30 to 45 km thick) Qinling-Dabie-Sulu orogenic belt (Assumpção et al. (2002); França & Assumpção (2004); Chen et al. (2010); Gao et al. (1998); Xu et al. (2013) respectively). The crustal velocity structure of these orogenic belts is also similar to the Scandinavian Caledonides. Neither shows a high velocity lower crustal layer at the base of the crust in contrast to the adjacent

18 *W. Ben Mansour et al. 2018*

shield/craton. These observations are consistent with a sharp Moho transition beneath the orogenic belts and a gradational transition beneath the shield.

This study and previous receiver function studies (Svenningsen et al. 2007; England & a 2012) show broadly consistent values of crustal thickness along the length of the Scandinavian mountains from north to south. Several seismic studies (Wawerzinek 2012; Frassetto & Thybo 2013; Maupin et al. 2013; Hejrani et al. 2015) have showed different properties of the lithosphere beneath the northern mountains and the southern mountains. From south to north, the lithosphere thickens, and has a decreasing  $V_p/V_s$  ratio suggesting increasing depletion. The consistency in crustal structure and variability in mantle structure was also noted by Ebbing & Olesen (2005) who modelled the variation the gravity anomaly across Scandinavia. They demonstrated that the northern mountains are supported by the distribution of mass in the upper crust and the southern mountains are supported by low density (depleted) lithospheric upper mantle.

This suggests that the mechanism of support for the southern and northern Scandinavian mountains is different. The new observations presented here provide an opportunity to test the hypothesis of Ebbing & Olesen (2005) that the northern Scandinavian mountains are supported by lateral variations in mass distribution in the upper crust. To do this three simple isostatic models have been constructed along a profile corresponding to the SCANLIPS2 profile and a profile parallel to the Atlantic coast. Assuming that the Caledonian orogen is predominantly reworked shield with relatively thin overlying nappes, average velocity values for the crust were converted to density using the relationship of Krasovsky (1981) for shields.

The resulting average density values for the crust are used in high density and low density end member models to test the isostatic support for the mountains provided by the crust. The results of this modelling is shown in figure 11. The high and low density end member models are effectively simple 1-D models of Airy isostatic support and do not take into account flexural rigidity. However, the mountains form a topographic load that has a length greater than 1000 km and a width of 500 km which is unlikely to be substantially supported by rigid shield crust. The small differences in depth to isostatic Moho between the high and low density models and the large uncertainty in the seismic Moho depth prevent critical testing of other models of support. The low density topography model is in effect a Pratt type model of isostatic compensation with lateral variations in crustal density being accommodated in the uppermost crust.

For each model, the Moho depth required to provide isostatic support for the mountains is shown and the Moho depths derived from the H-K stacking results along each profile is plotted for comparison. The Moho depth in the high and low density end member models is not significantly different (c.  $<2$  km). The low-density topography model requires a substantially thicker crust to provide sufficient support for the mountains. The uncertainties in the estimation of the Moho depth derived from H-k stacking prevent definitive conclusions to be drawn as to whether variations in crustal thickness support the mountains. However, the relationship between the calculated isostatic Moho depth and the Moho depths estimated from the seismic data are broadly consistent along both profiles with the high and low density models being closer to the seismic Moho than the low density topography model. This suggests that while variations in crustal thickness support the topography to a first order, the hypothesis of Ebbing & Olesen (2005) is supported by our data and lateral variations in near surface crustal density structure are responsible for supporting the mountains.

## CONCLUSION

P-receiver function analysis from two seismic broadband experiments (SCANLIPS2 and SCANLIPS3D), provides new information about the differences in crustal properties between the northern Scandinavian mountains and the Fennoscandian Shield. Using H-k stacking and interpolating the results, new maps of Moho depth and of Poisson's ratio have been produced for this region. The new results are in good agreement with previous studies and provide improved constraints where data were previously extrapolated from seismic refraction profiles. The main findings of this study are summarized in the following points:

- The crustal thickness varies between values of around 38 km close to the Atlantic coast to 48 to 49 km beneath the Fennoscandian shield.
- The contrast in velocity structure across the Moho (Moho sharpness) provides the clearest definition of the Caledonian orogen and the Fennoscandian shield domains, with the orogen being characterised by a sharp transition and the shield by a gradational transition.
- The gradient at the base of the shield is caused by the presence of a high velocity layer, most likely magmatic underplate. This layer is largely absent from beneath the orogen and was probably removed during orogenic reworking or during post-orogenic collapse.
- The contrast in physical properties of the crust at the transition from shield to orogenic belt is also observed in other regions, notably, Brazil and China, suggesting a common process is operating to rework the margins of shields involved in orogenic collisions.

20 W. Ben Mansour et al. 2018

- A simple 1D isostatic model cannot fully explain how the topography is supported across this region and lateral variations in crustal density structure must play a significant role.

## ACKNOWLEDGMENTS

We gratefully acknowledge support from the NERC geophysical equipment facility; loans 833 and 959, and the assistance of Jomar Gellein and Hasse Palm during the fieldwork. Financial support was provided by the Geological Survey of Norway. Parts of the data processing was undertaken using the SAC software (Goldstein & Snoke 2005) and figures were produced using GMT software (Wessel et al. 2013).

## REFERENCES

- Abbott, D. H., Mooney, W. D., & VanTongeren, J. A., 2013. The character of the Moho and lower crust within Archean cratons and the tectonic implications, *Tectonophysics*, **609**, 690–705.
- Åhäll, K.-I. & Larson, S. Å., 2000. Growth-related 1.85–1.55 Ga magmatism in the Baltic Shield; a review addressing the tectonic characteristics of Svecofennian, TIB 1-related, and Gothian events, *GFF*, **122**(2), 193–206.
- Ammon, C. J., 1991. The isolation of receiver effects from teleseismic P waveforms, *Bulletin of the Seismological Society of America*, **81**(6), 2504–2510.
- Ammon, C. J., Randall, G. E., & Zandt, G., 1990. On the non uniqueness of receiver function inversions, *Journal of Geophysical Research: Solid Earth*, **95**(B10), 15303–15318.
- Andersson, U. B., 1997. *Petrogenesis of Some Proterozoic Granitoid Suites and Associated Basic Rocks in Sweden: (geochemistry and Isotope Geology)*, Sveriges geologiska undersökning (SGU).
- Artemieva, I. M. & Thybo, H., 2013. EUNaseis: A seismic model for Moho and crustal structure in Europe, Greenland, and the North Atlantic region, *Tectonophysics*, **609**, 97–153.
- Assumpcao, M., James, D., & Snoke, A., 2002. Crustal thicknesses in SE Brazilian Shield by receiver function analysis: Implications for isostatic compensation, *Journal of Geophysical Research: Solid Earth (1978–2012)*, **107**(B1), ESE–2.
- Austrheim, H., Erambert, M., & Engvik, A. K., 1997. Processing of crust in the root of the Caledonian continental collision zone: the role of eclogitization, *Tectonophysics*, **273**(1), 129–153.
- Avedik, F., Berendsen, D., Fucke, H., Goldflam, S., Hirschleber, H., Meissner, R., Sellevoll, M., & Weinrebe, W., 1984. Seismic investigations along the Scandinavian Blue Norma profile, in *Annales geophysicae*, vol. 2, pp. 571–577, Gauthier-Villars.
- Barnes, C. G., Frost, C. D., Yoshinobu, A. S., McArthur, K., Barnes, M. A., Allen, C. M., Nordgulen, Ø., & Prestvik, T., 2007. Timing of sedimentation, metamorphism, and plutonism in the Helgeland Nappe Complex, north-central Norwegian Caledonides, *Geosphere*, **3**(6), 683–703.

## Crustal properties and teleseismic receiver functions 21

- Bostock, M., 2004. Green's functions, source signatures, and the normalization of teleseismic wave fields, *Journal of Geophysical Research: Solid Earth (1978–2012)*, **109**(B3).
- Cassidy, J., 1992. Numerical experiments in broadband receiver function analysis, *Bulletin of the Seismological Society of America*, **82**(3), 1453–1474.
- Chen, Y., Niu, F., Liu, R., Huang, Z., Tkalčić, H., Sun, L., & Chan, W., 2010. Crustal structure beneath China from receiver function analysis, *Journal of Geophysical Research: Solid Earth (1978–2012)*, **115**(B3).
- Chevrot, S. & van der Hilst, R. D., 2000. The Poisson's ratio of the Australian crust: geological and geophysical implications, *Earth and Planetary Science Letters*, **183**(1), 121–132.
- Christensen, N. & Mooney, W., 1995. Seismic velocity structure and composition of the continental crust: A global view, *Journal of Geophysical Research, Solid Earth*, (100), 9761–9788.
- Clayton, R. W. & Wiggins, R. A., 1976. Source shape estimation and deconvolution of teleseismic body waves, *Geophysical Journal International*, **47**(1), 151–177.
- Corne, D. W. & Knowles, J. D., 2007. Techniques for highly multi-objective optimisation: some non-dominated points are better than others, in *Proceedings of the 9th annual conference on Genetic and evolutionary computation*, pp. 773–780, ACM.
- Deb, K., Pratap, A., Agarwal, S., & Meyerivan, T., 2002. A fast and elitist multi-objective genetic algorithm: NSGA-II, *Evolutionary Computation, IEEE Transactions on*, **6**(2), 182–197.
- Ebbing, J. & Olesen, O., 2005. The northern and southern Scandes: structural differences revealed by an analysis of gravity anomalies, the geoid and regional isostasy, *Tectonophysics*, **411**(1), 73–87.
- Ebbing, J., Afework, Y., Olesen, O., & Nordgulen, Ø., 2005. Is there evidence for magmatic underplating beneath the Oslo rift?, *Terra Nova*, **17**(2), 129–134.
- England, R. W. & a, J., 2012. Crustal structure of central Norway and Sweden from integrated modelling of teleseismic receiver functions and the gravity anomaly, *Geophysical Journal International*, **191**(1), 1–11.
- Faleide, J. I., Kyrkjebø, R., Kjennerud, T., Gabrielsen, R. H., Jordt, H., Fanavoll, S., & Bjerke, M. D., 2002. Tectonic impact on sedimentary processes during Cenozoic evolution of the northern North Sea and surrounding areas, *Geological Society, London, Special Publications*, **196**(1), 235–269.
- França, G. S. & Assumpção, M., 2004. Crustal structure of the Ribeira fold belt, SE Brazil, derived from receiver functions, *Journal of South American Earth Sciences*, **16**(8), 743–758.
- Frassetto, A. & Thybo, H., 2013. Receiver function analysis of the crust and upper mantle in Fennoscandia—ostatic implications, *Earth and Planetary Science Letters*, **381**, 234–246.
- Gaál, G. & Gorbatshev, R., 1987. An outline of the Precambrian evolution of the Baltic Shield, *Precambrian Research*, **35**, 15–52.
- Gallagher, K., 2012. Uplift, denudation, and their causes and constraints over geological timescales, *Regional Geology and Tectonics: Principles of Geologic Analysis*, pp. 609–644.
- Gao, S., Luo, T.-C., Zhang, B.-R., Zhang, H.-F., Han, Y.-w., Zhao, Z.-D., & Hu, Y.-K., 1998. Chemical

22 W. Ben Mansour et al. 2018

- composition of the continental crust as revealed by studies in East China, *Geochimica et Cosmochimica Acta*, **62**(11), 1959–1975.
- Gee, D., Gorbatshev, R., & Ramberg, H., 1982. The Scandinavian Caledonides, *Profile of Orogenic Belts*, pp. 45–51.
- Goldstein, P. & Snoke, A., 2005. SAC availability for the IRIS community, *Incorporated Institutions for Seismology Data Management Center Electronic Newsletter*, **7**, 1–6.
- Gorbatshev, R. & Bogdanova, S., 1993. Frontiers in the Baltic shield, *Precambrian Research*, **64**(1), 3–21.
- Grad, M. & Luosto, U., 1987. Seismic models of the crust of the Baltic shield along the SVEKA profile in Finland, in *Annales geophysicae. Series B. Terrestrial and planetary physics*, vol. 5, pp. 639–649.
- Grad, M., Tiira, T., et al., 2009. The Moho depth map of the European plate, *Geophysical Journal International*, **176**(1), 279–292.
- Grenne, T., Ihlen, P., & Vokes, F., 1999. Scandinavian Caledonide metallogeny in a plate tectonic perspective, *Mineralium Deposita*, **34**(5-6), 422–471.
- Guggisberg, B., Kaminski, W., & Prodehl, C., 1991. Crustal structure of the Fennoscandian Shield: A travelttime interpretation of the long-range FENNOLORA seismic refraction profile, *Tectonophysics*, **195**(2), 105–137.
- Hansen, P. C., 1992. Analysis of discrete ill-posed problems by means of the L-curve, *SIAM review*, **34**(4), 561–580.
- Hejrani, B., Balling, N., Jacobsen, B., & England, R., 2015. Upper-mantle velocities below the Scandinavian mountains from P- and S-wave travelttime tomography, *Tectonophysics*.
- Hirschleber, H., Lund, C., Meissner, R., Vogel, A., & Weinrebe, W., 1975. Seismic investigations along the Scandinavian Blue Road traverse, *J. Geophys.*, **41**(2), 135–148.
- Högdahl, K., Andersson, U. B., & Eklund, O., 2004. *The Transscandinavian Igneous Belt (TIB) in Sweden: a review of its character and evolution*, vol. 37, Geological survey of Finland Espoo.
- Hollocher, K., Robinson, P., Walsh, E., & Roberts, D., 2012. Geochemistry of amphibolite-facies volcanics and gabbros of the Støren Nappe in extensions west and southwest of Trondheim, Western Gneiss Region, Norway: a key to correlations and paleotectonic settings, *American Journal of Science*, **312**(4), 357–416.
- Hossain, M. et al., 1989. Seismic refraction studies in the Baltic Shield along the FENNOLORA profile.
- Hughes, S., Luetgert, J., & Christensen, N., 1993. Reconciling deep seismic refraction and reflection data from the Grenvillian-Appalachian boundary in western New England, *Tectonophysics*, **225**(4), 255–269.
- Hyvönen, T., Tiira, T., Korja, A., Heikkinen, P., & Rautioaho, E., 2007. A tomographic crustal velocity model of the central Fennoscandian Shield, *Geophysical Journal International*, **168**(3), 1210–1226.
- Kelly, A., England, R. W., & Maguire, P. K., 2007. A crustal seismic velocity model for the UK,

- Ireland and surrounding seas, *Geophysical Journal International*, **171**(3), 1172–1184.
- Kennett, B., 1983. Seismic wave propagation in stratified media, *Pres.*, Cambridge.
- Koistinen, T., Stephens, M., Bogatchev, V., Nordgulen, Ø., Wennerstrøm, M., & Korhonen, J., 2001. Geological map of the Fennoscandian Shield, scale 1: 2 million, *Geological Surveys of Finland, Norway and Sweden and North-West Department of Natural Resources of Russia*.
- Kolstrup, M. L. & Maupin, V., 2013. A Proterozoic boundary in southern Norway revealed by joint-inversion of P-receiver functions and surface waves, *Precambrian Research*, **238**, 186–198.
- Korja, A., Lahtinen, R., & Nironen, M., 2006. The Svecofennian orogen: a collage of microcontinents and island arcs, *Geological Society, London, Memoirs*, **32**(1), 561–578.
- Korsman, K., Korja, T., Pajunen, M., Virransalo, P., working group, G., et al., 1999. The GGT/SVEKA transect: structure and evolution of the continental crust in the Paleoproterozoic Svecofennian orogen in Finland, *International Geology Review*, **41**(4), 287–333.
- Kozlovskaya, E., Kosarev, G., Aleshin, I., Riznichenko, O., & Sanina, I., 2008. Structure and composition of the crust and upper mantle of the Archean–Proterozoic boundary in the Fennoscandian shield obtained by joint inversion of receiver function and surface wave phase velocity of recording of the SVEKALAPKO array, *Geophysical Journal International*, **175**(1), 135–152.
- Krasovsky, S., 1981. Reflection of continental-type crustal dynamics in the gravity field, *Navukova Dumka, Kiev*.
- Kukkonen, I., Kuusisto, M., Lehtonen, M., & Peltonen, P., 2008. Delamination of eclogitized lower crust: control on the crust–mantle boundary in the central Fennoscandian shield, *Tectonophysics*, **457**(3), 111–127.
- Lahtinen, R., 1994. *Crustal evolution of the Svecofennian and Karelian domains during 2.1–1.79 Ga, with special emphasis on the geochemistry and origin of 1.93–1.91 Ga gneissic tonalites and associated supracrustal rocks in the Rautalampi area, central Finland*, vol. 378, Geological tutkimuskeskus.
- Langston, C. A., 1979. Structure under Mount Rainier, Washington, inferred from teleseismic body waves, *Journal of Geophysical Research: Solid Earth (1978–2012)*, **84**(B9), 4749–4762.
- Laske, G., Masters, G., Ma, Z., & Pasyanos, M., 2013. Update on CRUST1.0 - A 1-degree global model of Earth's crust, in *Geophys. Res. Abstracts*, vol. 15, p. 2658.
- Levin, V. & Park, J., 1997. Crustal anisotropy in the Ural mountains foredeep from teleseismic receiver functions, *Geophysical research letters*, **24**(11), 1283–1286.
- Lombardi, D., Braunmiller, J., Kissling, E., & Giardini, D., 2008. Moho depth and Poisson's ratio in the Western-Central Alps from receiver functions, *Geophysical Journal International*, **173**(1), 249–264.
- Lund, C.-E., 1979. Crustal structure along the Blue Road profile in northern Scandinavia, *GFF*, **101**(3), 191–204.
- Luosto, U., 1997. Structure of the Earth's crust in Fennoscandia as revealed from refraction and wide-angle reflection studies, *Geophysica*, **33**(1), 3–16.
- Luosto, U., Lanne, E., Korhonen, H., Guterch, A., Grad, M., Materzok, R., & Perchuc, E., 1984. Deep

- structure of the Earth's crust on the SVEKA profile in central Finland, in *Annales geophysicae*, vol. 2, pp. 559–570, Gauthier-Villars.
- Luosto, U., Flueh, E., & Lund, C.-E., 1989. The crustal structure along the POLAR profile from seismic refraction investigations, *Tectonophysics*, **162**(1), 51–85.
- Luosto, U., Tiira, T., Korhonen, H., Azbel, I., Burmin, V., Buyanov, A., Kosminskaya, I., Ionkis, V., & Sharov, N., 1990. Crust and upper mantle structure along the DSS Baltic profile in SE Finland, *Geophysical Journal International*, **101**(1), 89–110.
- Mänttari, I. & Hölttä, P., 2002. U–Pb dating of zircons and monazites from Archean granulites in Varpaisjärvi, Central Finland: Evidence for multiple metamorphism and Neoproterozoic terrane accretion, *Precambrian Research*, **118**(1), 101–131.
- Maupin, V., Agostini, A., Artemieva, I., Balling, N., Beekman, F., Ebbing, J., England, R., Frassetto, A., Gradmann, S., Jacobsen, B., et al., 2013. The deep structure of the Scandes and its relation to tectonic history and present-day topography, *Tectonophysics*, **602**, 15–37.
- Mikkola, P., Huhma, H., Heilimo, E., & Whitehouse, M., 2011. Archean crustal evolution of the Suomussalmi district as part of the Kianta Complex, Karelia: constraints from geochemistry and isotopes of granitoids, *Lithos*, **125**(1), 287–307.
- Moorkamp, M., Jones, A., & Fishwick, S., 2010. Joint inversion of receiver functions, surface wave dispersion, and magnetotelluric data, *Journal of Geophysical Research: Solid Earth (1978–2012)*, **115**(B4).
- Musacchio, G., Mooney, W. D., Luetgert, J. H., & Christensen, N. I., 1997. Composition of the crust in the Grenville and Appalachian Provinces of North America inferred from Vp/Vs ratios, *Journal of Geophysical Research: Solid Earth (1978–2012)*, **102**(B7), 15225–15241.
- Mykkeltveit, S., 1980. A seismic profile in southern Norway, *Pure and Applied Geophysics*, **118**(2), 1310–1325.
- Nironen, M., 1997. The Svecofennian Orogen: a tectonic model, *Precambrian Research*, **86**(1), 21–44.
- Niu, F. & James, D. E., 2002. Fine structure of the lowermost crust beneath the Kaapvaal craton and its implications for crustal formation and evolution, *Earth and Planetary Science Letters*, **200**(1), 121–130.
- Olesen, O., Lundin, E., Nordgulen, O., Osmundsen, P. T., Skilbrei, J. R., Smethurst, M. A., Solli, A., Bugge, T., & Fichler, C., 2002. Bridging the gap between the onshore and offshore geology in Nordland, northern Norway, *Norsk geologisk tidsskrift*, **82**(4), 243–262.
- Olesen, O., Brønner, M., Ebbing, J., Gellein, J., Gernigon, L., Koziel, J., Lauritsen, T., Myklebust, R., Pascal, C., Sand, M., et al., 2010. New aeromagnetic and gravity compilations from Norway and adjacent areas: methods and applications, in *Geological Society, London, Petroleum Geology Conference series*, vol. 7, pp. 559–586, Geological Society of London.
- Olsson, S., Roberts, R. G., & Bødvarsson, R., 2008. Moho depth variation in the Baltic Shield from analysis of converted waves, *Gff*, **130**(3), 113–122.
- Ottmøller, L. & Midzi, V., 2003. The crustal structure of Norway from inversion of teleseismic

*Crustal properties and teleseismic receiver functions* 25

- receiver functions, *Journal of seismology*, **7**(1), 35–48.
- Owens, T. J., Zandt, G., & Taylor, S. R., 1984. Seismic evidence for an ancient rift beneath the Cumberland Plateau, Tennessee: A detailed analysis of broadband teleseismic P waveforms, *Journal of Geophysical Research: Solid Earth (1978–2012)*, **89**(B9), 7783–7795.
- Platt, J., 1993. Exhumation of high-pressure rocks: A review of concepts and processes, *Terra nova*, **5**(2), 119–133.
- Prodehl, C. & Kaminski, W., 1984. Crustal structure under the FENNOLOGRA profile, in *First EGT Workshop: The Northern Segment*, pp. 43–48, European Science Foundation Strasbourg.
- Roberts, D. & Gee, D. G., 1985. An introduction to the structure of the Scandinavian Caledonides, *The Caledonide orogen–Scandinavia and related areas*, **1**, 55–68.
- Roberts, D., Nordgulen, Ø., & Melezhik, V., 2007. The uppermost allochthon in the Scandinavian Caledonides: From a Laurentian ancestry through Taconian orogeny to Scandian crustal growth on Baltica, *Geological Society of America Memoirs*, **200**, 357–377.
- Savage, M. K., 1998. Lower crustal anisotropy or dipping boundaries? Effects on receiver functions and a case study in New Zealand, *Journal of Geophysical Research: Solid Earth (1978–2012)*, **103**(B7), 15069–15087.
- Sellevoll, M. A. & Penttilä, E., 1964. *Seismic refraction measurements of crustal structure in Northern Scandinavia*, Norwegian universities Press.
- Silvennoinen, H., Kozlovskaya, E., Kissling, E., Kosarev, G., Working Group, P., et al., 2014. A new Moho boundary map for the northern Fennoscandian Shield based on combined controlled-source seismic and receiver function data, *GeoResJ*, **1**, 19–32.
- Stephens, M. & Gee, D., 1985. A tectonic model for the evolution of the eugeoclinal terranes in the central Scandinavian Caledonides, *The Caledonide Orogen: Scandinavia and Related Areas*. Wiley, Chichester, pp. 953–978.
- Stephens, M. B. & Gee, D. G., 1989. Terranes and polyphase accretionary history in the Scandinavian Caledonides, *Geological Society of America Special Papers*, **230**, 17–30.
- Stratford, W. & Thybo, H., 2011. Seismic structure and composition of the crust beneath the southern Scandes, Norway, *Tectonophysics*, **502**(3), 364–382.
- Stratford, W., Thybo, H., Faleide, J. I., Olesen, O., & Tryggvason, A., 2009. New Moho map for onshore southern Norway, *Geophysical Journal International*, **178**(3), 1755–1765.
- Svenningsen, L., Balling, N., Jacobsen, B., Kind, R., Wylegalla, K., & Schweitzer, J., 2007. Crustal root beneath the highlands of southern Norway resolved by teleseismic receiver functions, *Geophysical Journal International*, **170**(3), 1129–1138.
- Tesauro, M., Kaban, M. K., & Cloetingh, S. A., 2008. EuCRUST-07: A new reference model for the European crust, *Geophysical Research Letters*, **35**(5).
- Thompson, D., Bastow, I., Helffrich, G., Kendall, J., Wookey, J., Snyder, D., & Eaton, D., 2010. Precambrian crustal evolution: seismic constraints from the Canadian shield, *Earth and Planetary*

26 W. Ben Mansour et al. 2018

*Science Letters*, **297**(3), 655–666.

Thurner, S., Margolis, R., Levander, A., & Niu, F., 2015. PdS receiver function evidence for crustal scale thrusting, relic subduction, and mafic underplating in the Trans-Hudson Orogen and Yavapai province, *Earth and Planetary Science Letters*, **426**, 13–22.

Thybo, H., 2001. Crustal structure along the EGT profile across the Tornquist Fan interpreted from seismic, gravity and magnetic data, *Tectonophysics*, **334**(3), 155–190.

Vinnik, L., 1977. Detection of waves converted from P to Sv in the mantle, *Physics of the Earth and planetary interiors*, **15**(1), 39–45.

Wang, X.-Q., Schubnel, A., Fortin, J., David, E., Guéguen, Y., & Ge, H.-K., 2012. High Vp/Vs ratio: Saturated cracks or anisotropy effects?, *Geophysical Research Letters*, **39**(11).

Watanabe, T., 1993. Effects of water and melt on seismic velocities and their application to characterization of seismic reflectors, *Geophysical Research Letters*, **20**(24), 2933–2936.

Wawerzinek, B., 2012. *Untersuchung der elastischen Scherwellenstruktur unter dem Sdskandinavischen Gebirge*, Ph.D. thesis, Karlsruhe, Karlsruher Institut für Technologie (KIT), Diss., 2012.

Weinrebe, W., 1981. Joint interpretation of earthquake travel-time residuals and seismic measurements along the Blue Norma profile in northern Scandinavia, *Pure and Applied Geophysics*, **119**(6), 1107–1115.

Wessel, P., Smith, W. H., Scharroo, R., Luis, J., & Wobbe, F., 2013. Generic Mapping Tools: improved version released, *Eos, Transactions American Geophysical Union*, **94**(45), 409–410.

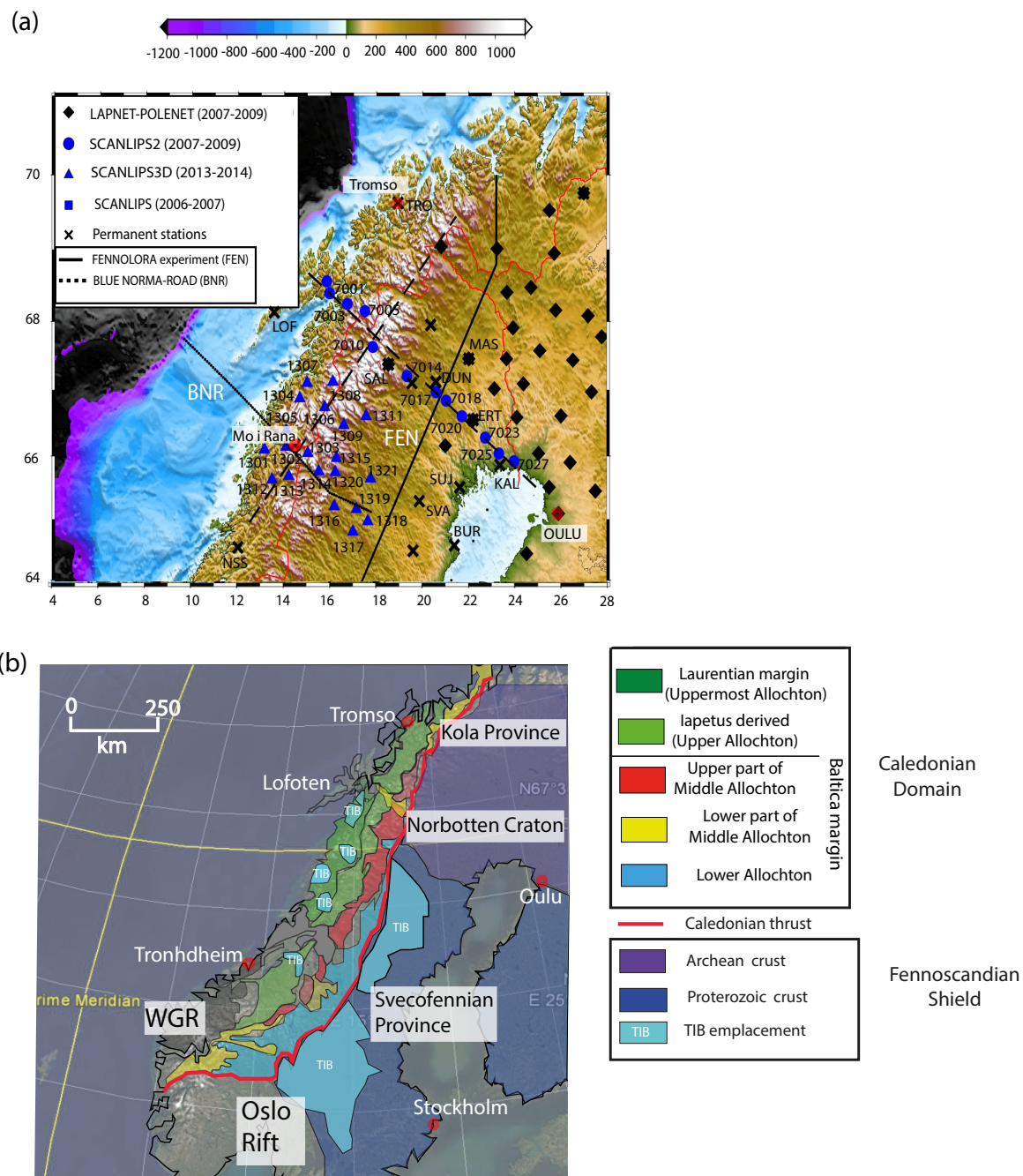
Xu, Q., Zhao, J., Pei, S., & Liu, H., 2013. Distinct lateral contrast of the crustal and upper mantle structure beneath northeast Tibetan plateau from receiver function analysis, *Physics of the Earth and Planetary Interiors*, **217**, 1–9.

Youssof, M., Thybo, H., Artemieva, I., & Levander, A., 2013. Moho depth and crustal composition in southern Africa, *Tectonophysics*, **609**, 267–287.

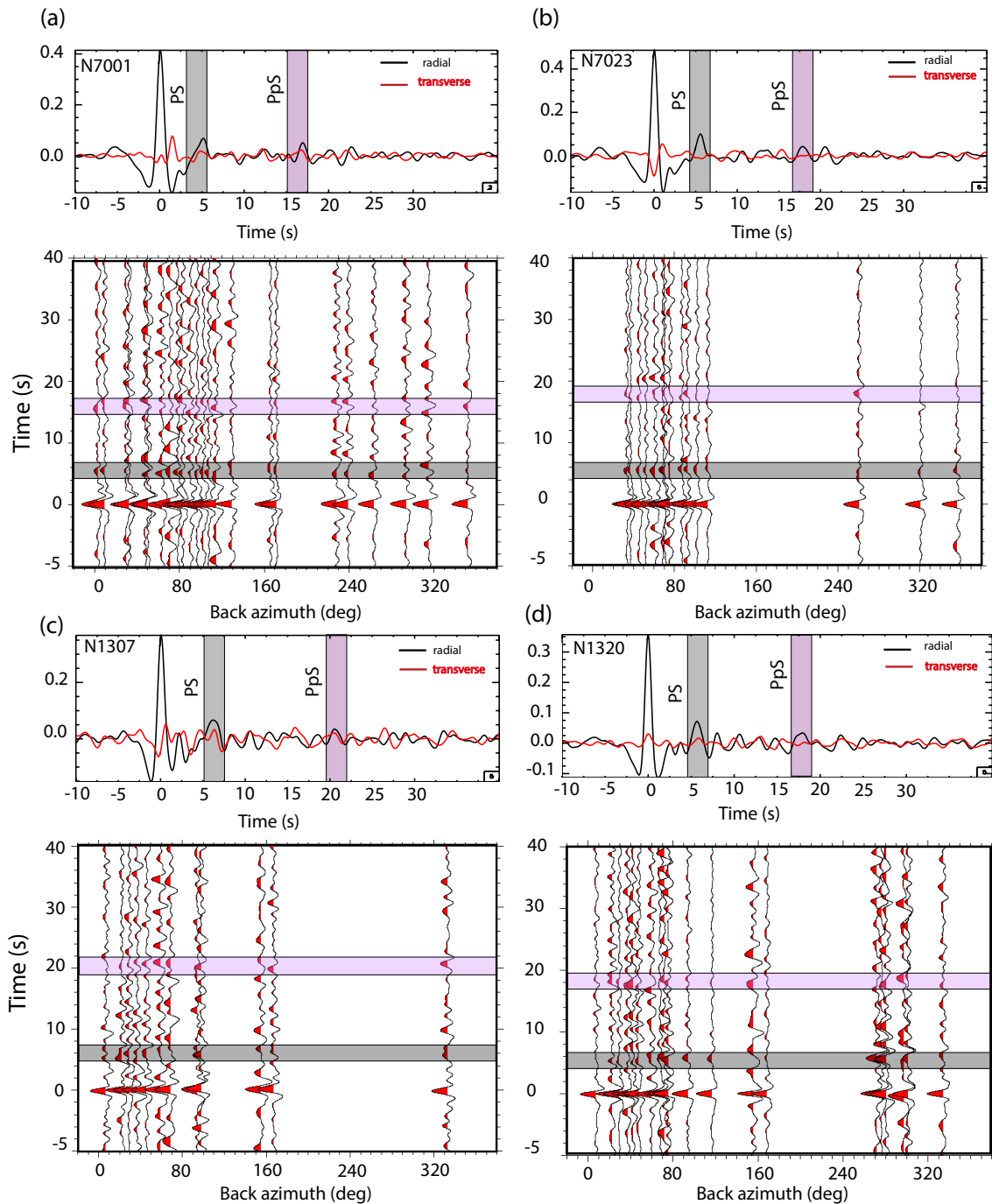
Zandt, G. & Ammon, C. J., 1995. Continental crust composition constrained by measurements of crustal Poisson's ratio, *Nature*, **374**(6518), 152–154.

Zhu, L., 2000. Crustal structure across the San andreas Fault, southern California from teleseismic converted waves, *Earth and Planetary Science Letters*, **179**(1), 183–190.

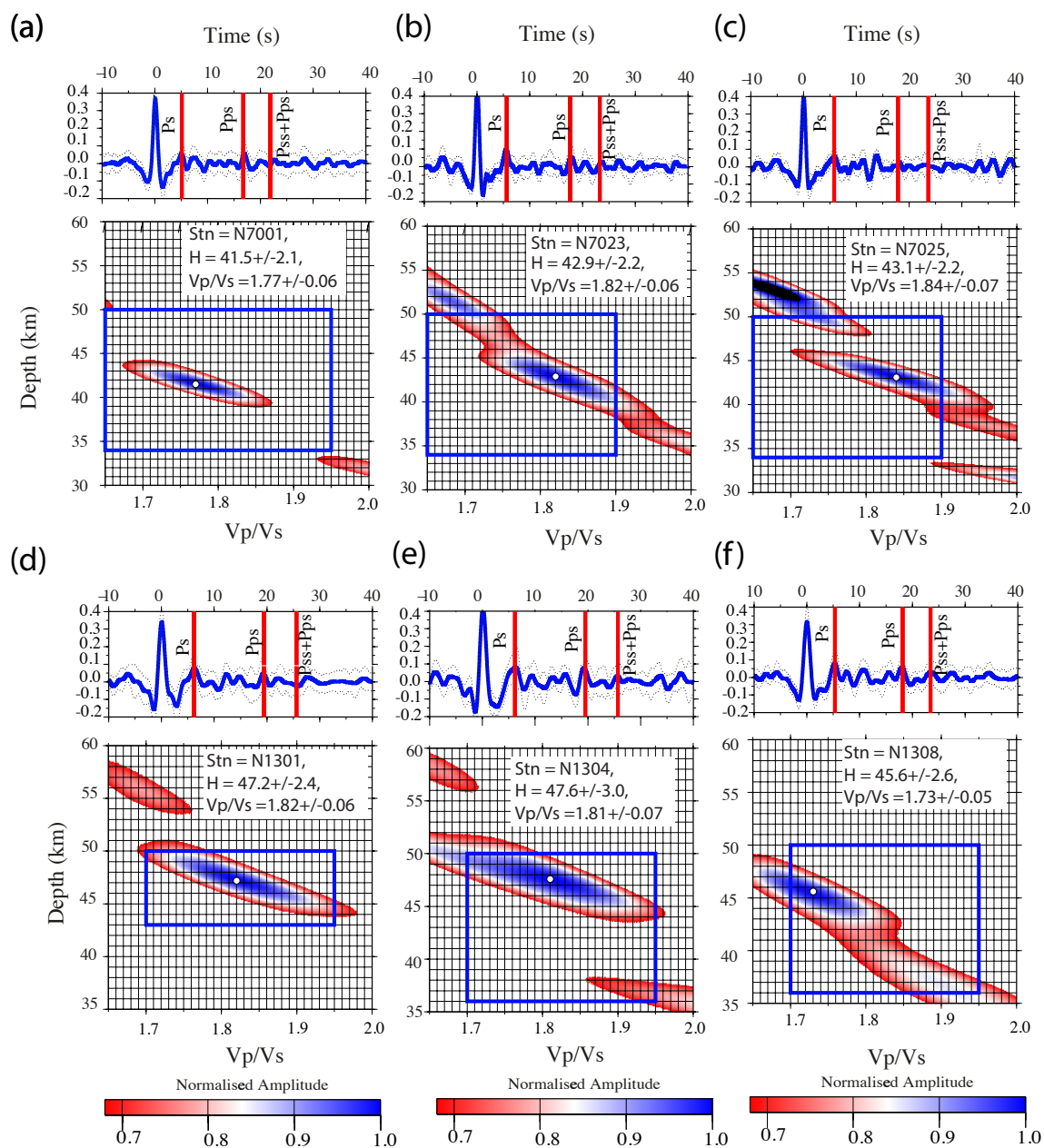
Zhu, L. & Kanamori, H., 2000. Moho depth variation in southern California from teleseismic receiver functions, *Journal of Geophysical Research: Solid Earth (1978–2012)*, **105**(B2), 2969–2980.



**Figure 1.** (a) Map showing topography of Scandinavia and the location of seismic experiments across the Northern Scandinavian Mountains. (b) Simplified geological map based on Koistinen et al. (2001) of the Scandinavian Peninsula. WGR: Western Gneiss Region; TIB: Trans-Scandinavian Igneous Belt.

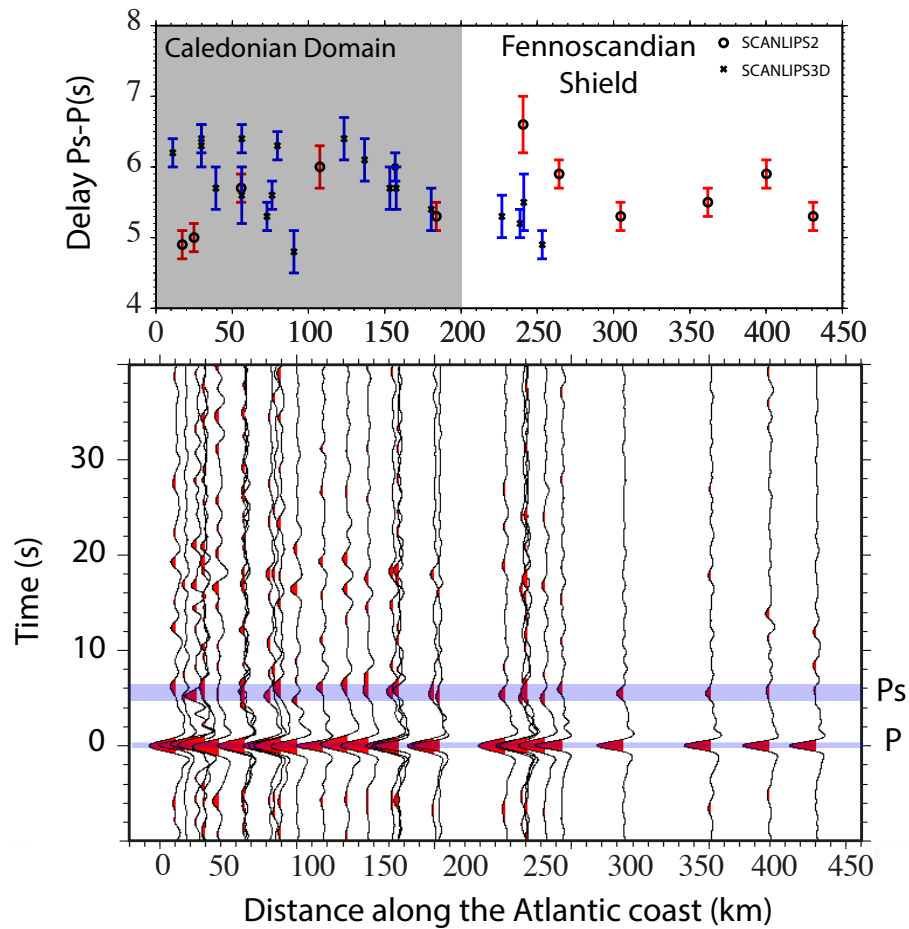
28 *W. Ben Mansour et al. 2018*

**Figure 2.** Examples of radial P-receiver functions computed for 2 stations of the SCANLIPS2 experiment (a and b) and 2 stations of the SCANLIPS3D experiment (c and d): Top: A stack of all receiver functions together with the stack of the associated transverse receiver functions are presented. Ps conversion and PpS conversions are marked in grey and purple on these plots. Bottom: P-receiver functions are presented sorted by backazimuth.

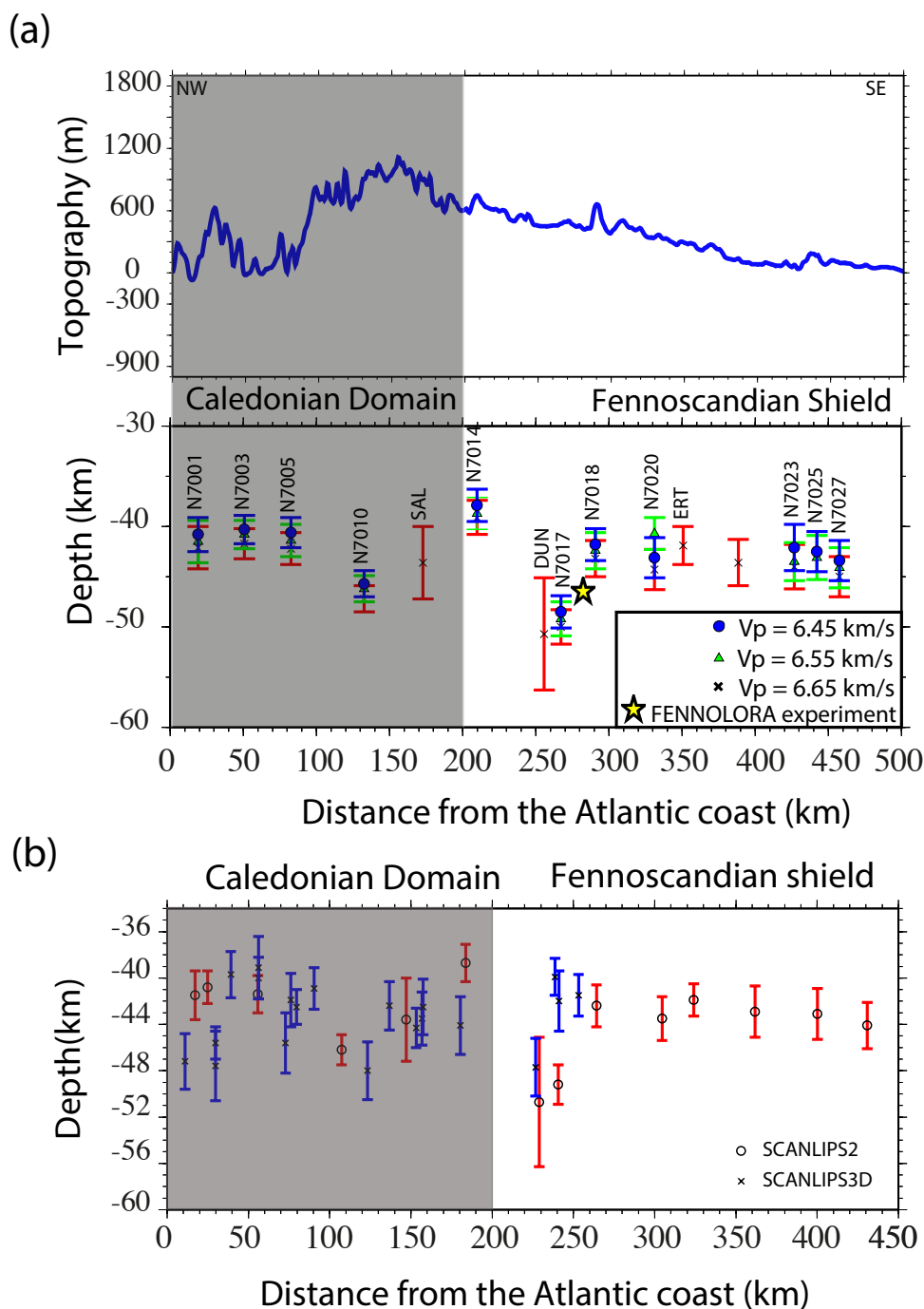


**Figure 3.** Examples of H-k stacking for 3 stations from SCANLIPS2 (a to c) and 3 stations from SCANLIPS3D (d to f). Top: the stack P-receiver functions with phases converted (Ps, Pps and Pss) picked and bottom, the grid search in domain Depth- $V_p/V_s$ . The blue square corresponds to the area where amplitudes of each phase are normalised and the white dot corresponds to the best couple Depth- $V_p/V_s$ .

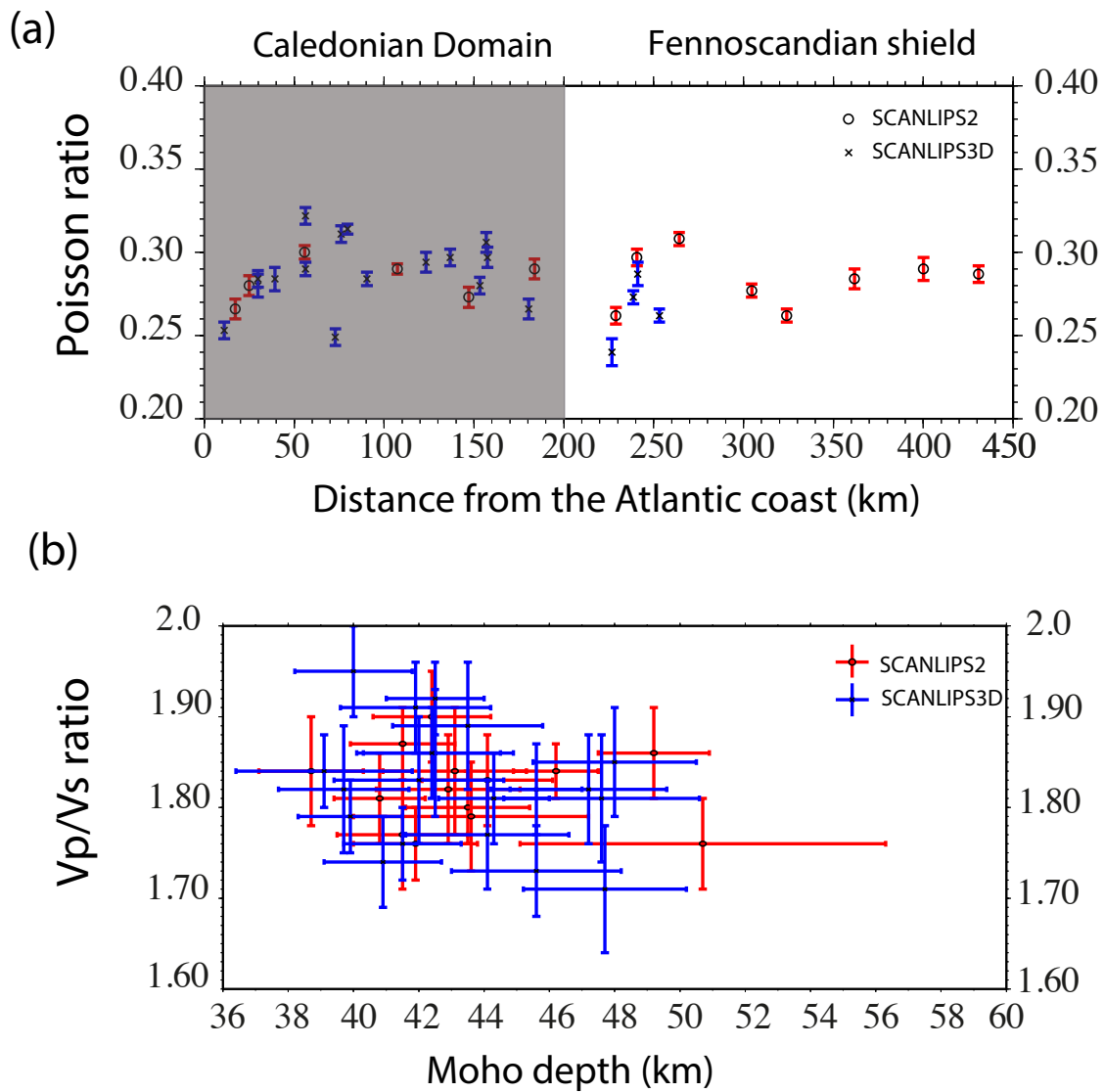
30 *W. Ben Mansour et al. 2018*



**Figure 4.** Top: Longitudinal variation of delay between the Ps conversion and the direct P wave arrival beneath the SCANLIPS2 experiment between latitudes  $65.9^{\circ}$  N and  $69.5^{\circ}$  N (black circles) and the SCANLIPS3D experiment between latitudes  $64.5^{\circ}$  N and  $67.5^{\circ}$  N (black crosses). Bottom: Longitudinal variation of stacked P-receiver functions associated above. The arrival time of the direct P wave and Ps conversion is highlighted in pale blue.



**Figure 5.** (a) Variation in Moho depth along the SCANLIPS2 experiment for 3 different values of  $V_p$  ( $6.45 \text{ km s}^{-1}$ ,  $6.55 \text{ km s}^{-1}$  and  $6.65 \text{ km s}^{-1}$ ) between latitudes  $65.9^\circ \text{ N}$  and  $69.5^\circ \text{ N}$ . The topography along the profile is shown in the top panel. The Caledonian domain is delimited in grey on these plots. Indicated with a yellow star is the Moho depth estimated from the FENNOLORA experiment between shots F and G. (b) Comparison of longitudinal variation of Moho depth between the SCANLIPS2 experiment (black circles) and the SCANLIPS3D experiments (black crosses) for  $V_p = 6.55 \text{ km.s}^{-1}$ .

32 *W. Ben Mansour et al. 2018*

**Figure 6.** (a) Longitudinal variation of Poisson's ratio beneath the SCANLIPS2D experiments between latitudes 65.9° N and 69.5° N (black circles) and the SCANLIPS3D experiments between latitudes 64.5° N and 67.5° N (black crosses). (b) Variation of Moho depth with Vp/Vs ratio in the study area.

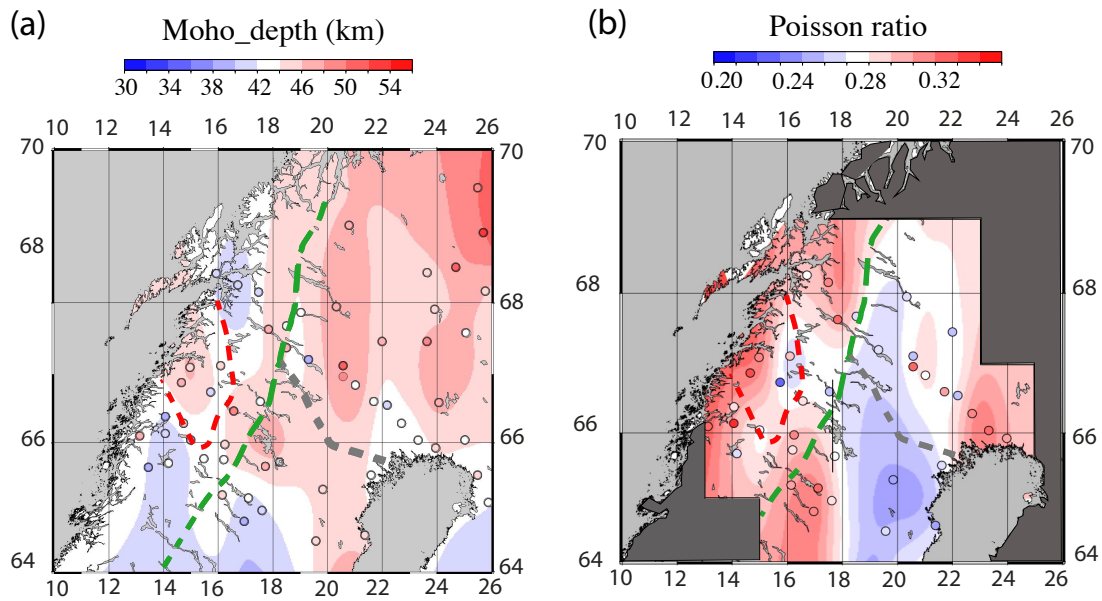


**Figure 7.** (a) Moho depth, (b) Poisson's ratio. Indicated in the green dashed line is the Caledonian thrust between the Fennoscandian shield and the Caledonian domain and in the grey dashed line the limit between Archean crust and Proterozoic crust. Both maps created using gridding with continuous curvature splines with a tension factor  $T = 0.4$  from the compilation of data of the SCANLIPS2 experiment, the SCANLIPS3D experiment, the LAPNET-POLENET experiment (Silvennoinen et al. 2014) and the Swedish National Seismic Network (Olsson et al. 2008).

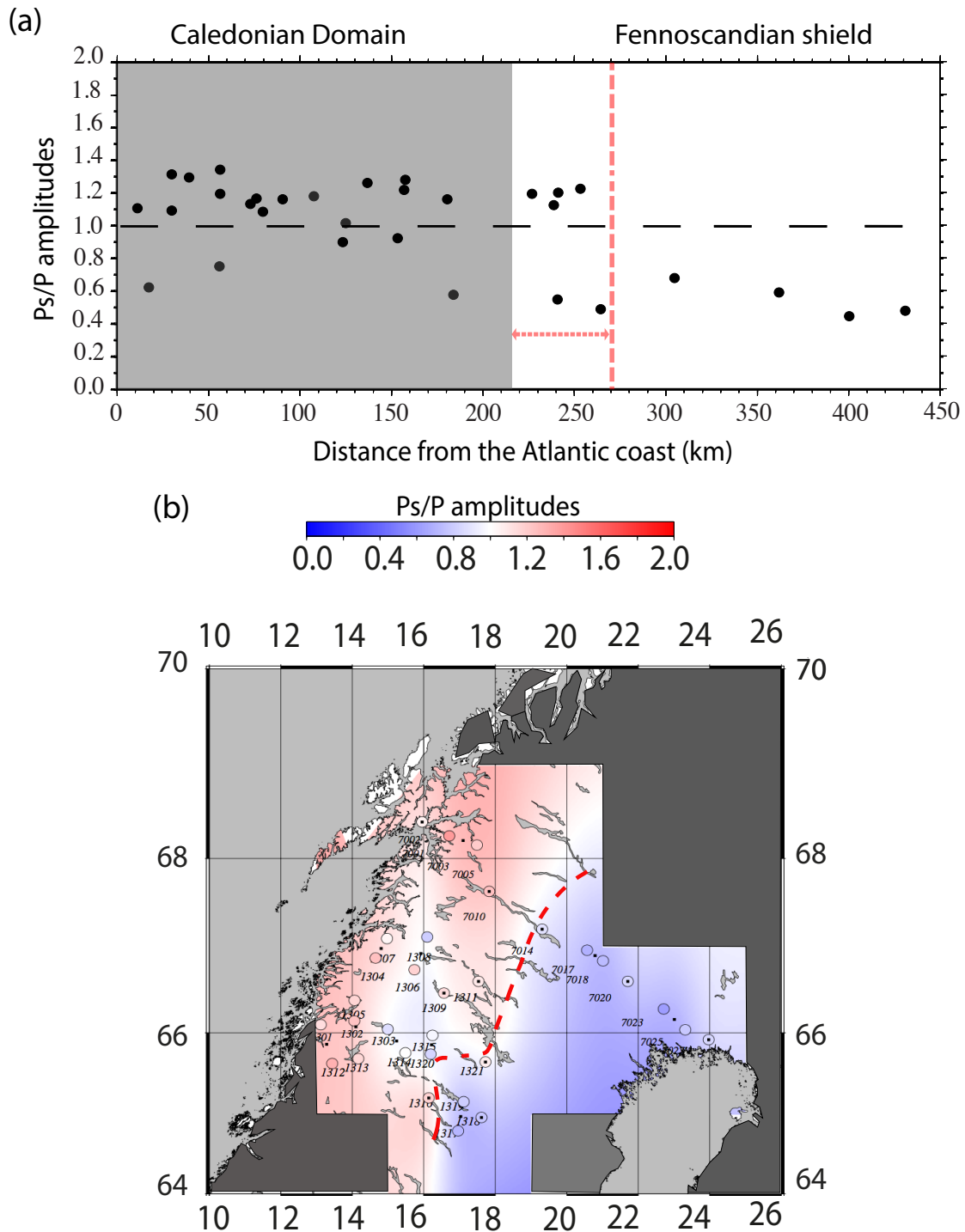


**Figure 8.** (a) Longitudinal variation of Moho sharpness beneath the SCANLIPS2D experiment between latitudes  $65.9^{\circ}$  N and  $69.5^{\circ}$  N and the SCANLIPS3D experiment between latitudes  $64.5^{\circ}$  N and  $69^{\circ}$  N. Indicated in red is the limit between a domain with  $R > 1$  and a domain with  $R < 1$ . (b) 2D Moho sharpness map for an average slowness  $p=0.060^{\circ}/s$  using a gridding with continuous curvature splines with a tension factor  $T=0.4$ . Data are compiled from the SCANLIPS2 experiment and the SCANLIPS3D experiment (dots on the map). Indicated in red is the limit between a domain with  $R > 1$  and a domain with  $R < 1$ .

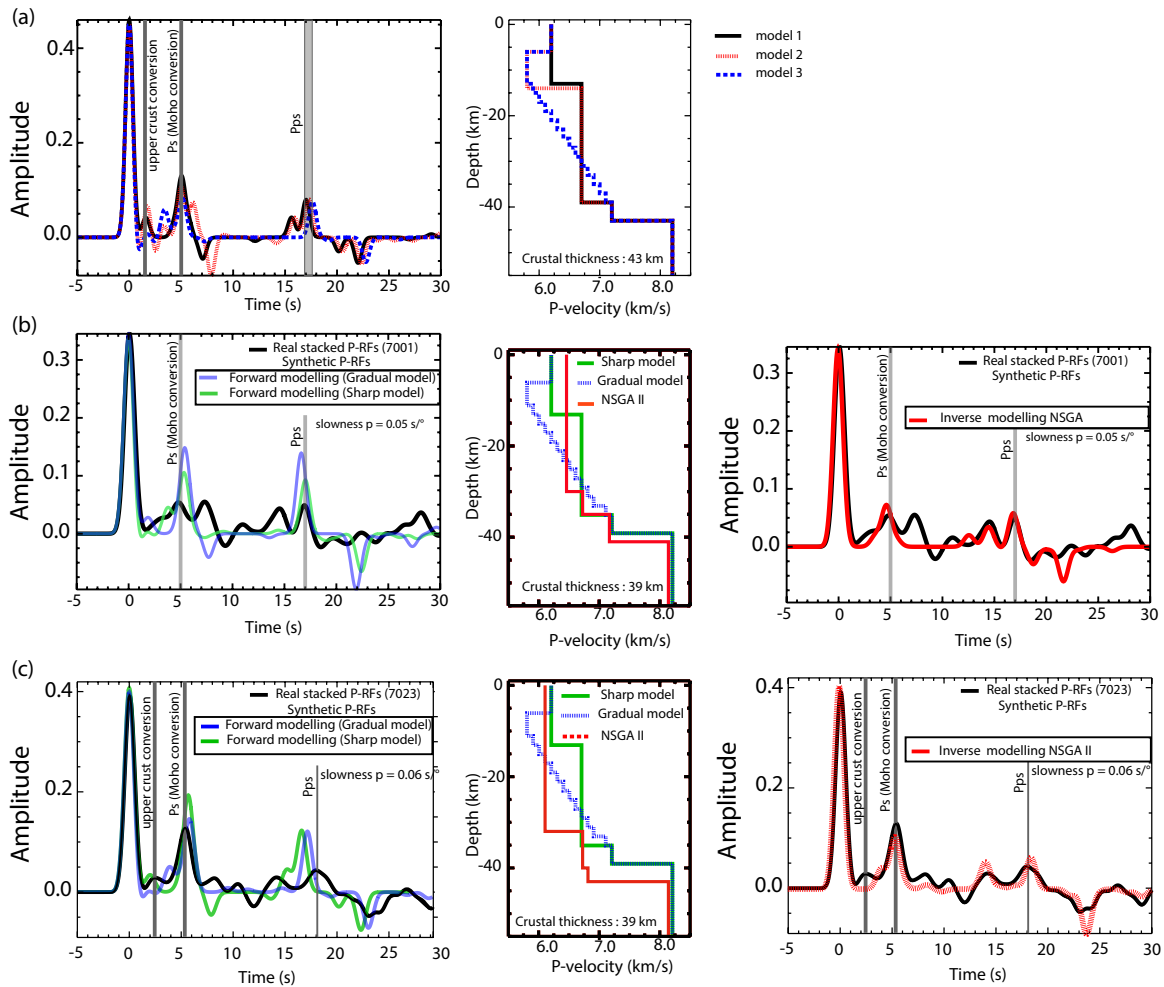


**Figure 9.** (a) Synthetic receiver functions for 3 existing crustal models for Scandinavia derived from forward modelling (model 1: FENNOLORA profile, model 2: model with a low velocity zone at the base of the upper crust as suggested by Ottemöller & Midzi (2003), model 3: model with a gradual transition between the upper crust and Moho). Ps, PpS conversions are picked and also the upper crust conversion. (b) Comparison of stacked P-receiver functions (in black) with a synthetic P-receiver function derived from forward modelling for a model with a sharp Moho (in green) and a model with a gradual Moho (in blue) for a station located in the Caledonian domain ((b), station 7001) and a station located on the Fennoscandian shield ((c), station 7023). Ps, PpS conversions are picked on the plot.

36 *W. Ben Mansour et al. 2018*

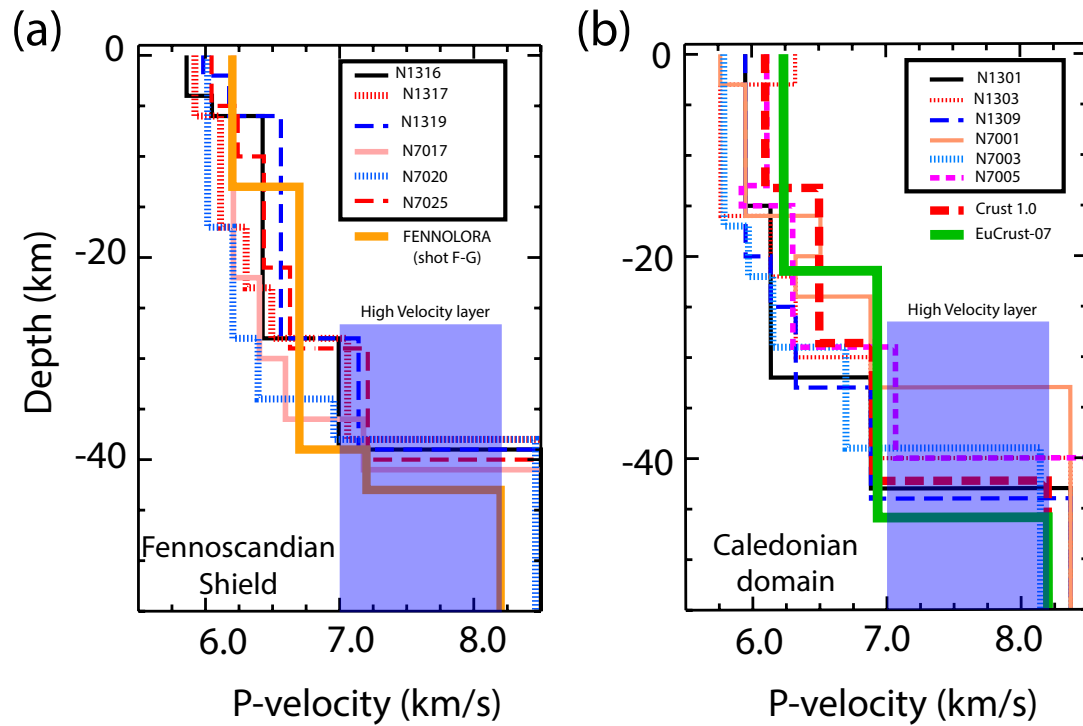


**Figure 10.** (a) Comparison of a 1D crustal model derived from P-receiver functions beneath the Fennoscandian shield with a crustal model from the FENNOLORA seismic refraction profile (shots F-G: orange line). (b) Comparison of a 1D crustal model derived from P-receiver functions beneath the Caledonian orogen with the global crustal model CRUST 1.0 (red dashed line, Laske et al. (2013)) and EuCRUST07 (green line, Tesauro et al. (2008)).

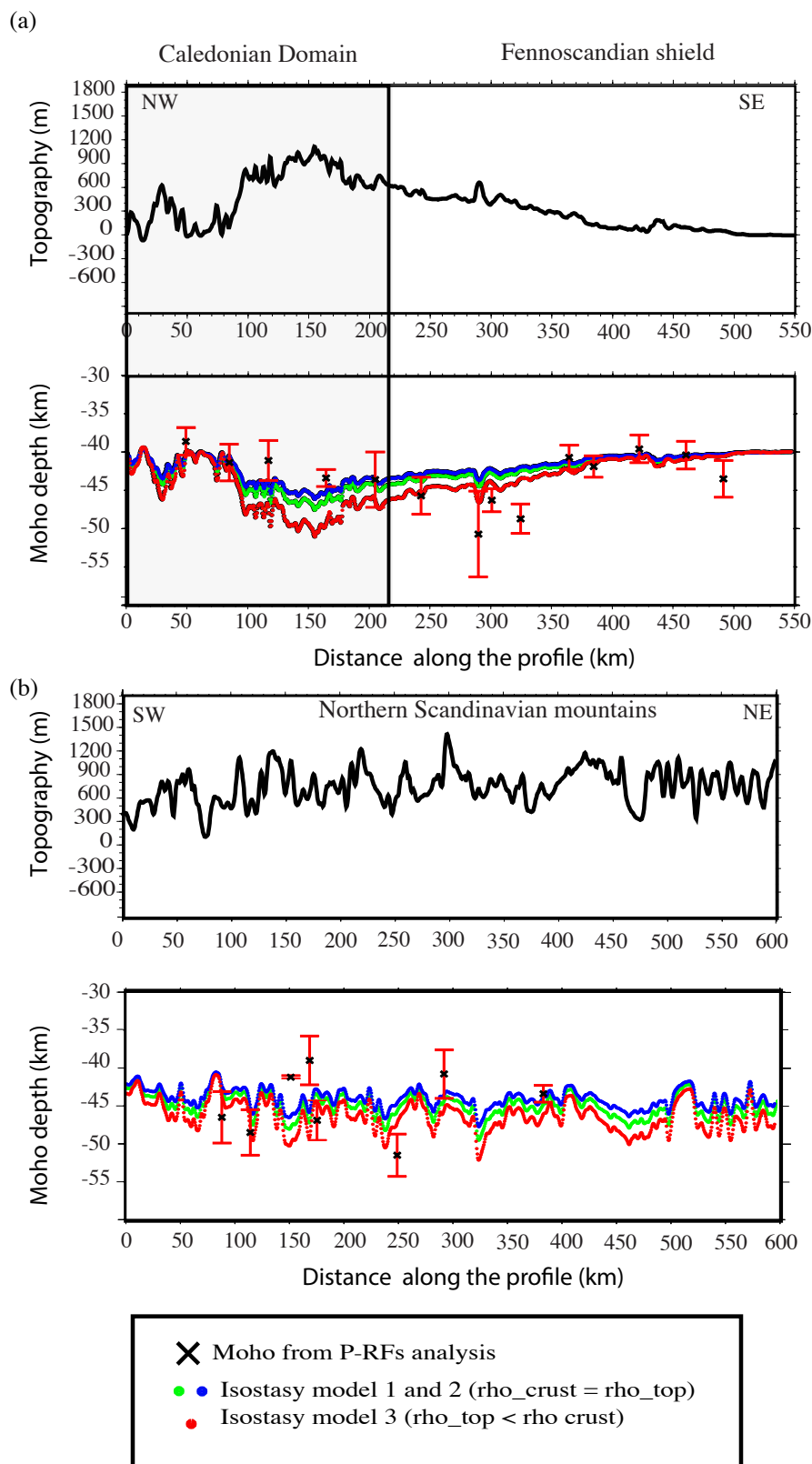


**Figure 11.** Comparison of Moho depths predicted for different crustal densities by an Airy isostatic model (colored dots) and the Moho depth calculated from P-receiver functions analysis (black crosses) along the SCANLIPS2 experiment. 3 isostatic models are used here: a model with an average crustal density  $2813 \text{ kg m}^{-3}$  (green line), a model with an average crustal density  $2700 \text{ kg m}^{-3}$  (blue line) and a model with  $2670 \text{ kg m}^{-3}$  for the topography and  $2950 \text{ kg m}^{-3}$  for the crust (red line).